First-principles nonlocal-pseudopotential approach in the density-functional formalism. II. Application to electronic and structural properties of solids

Alex Zunger* and Marvin L. Cohen
Department of Physics, University of California and Materials and Molecular Research Division, Lawrence Berkeley Laboratory, Berkeley, California 94720
(Received 7 August 1978; revised manuscript received 21 August 1979)

We apply our previously developed first-principles nonlocal pseudopotentials (obtained for all atoms of rows 1–5 in the Periodic Table) to study self-consistently the electronic structure of Si and Ge and the transition metals Mo and W. For Si and Ge we find that the first-principles pseudopotentials yield valence-band states in good agreement with the empirically adjusted pseudopotential and photoemission data, whereas the low conduction-band states appear to be consistently lower in energy due apparently to incomplete cancellation of the self-interaction effects. The calculated x-ray scattering factors (obtained by core orthogonalization of the pseudo-wave-functions) are in excellent agreement with experiment. The self-consistent valence charge density shows a distinct elongation of the covalent bond along the internuclear axis, in good agreement with the experimentally synthesized density. The systematic deviations of the empirical pseudopotential results from the present are discussed in terms of the underlying differences in the potentials in the high-momentum regions. Using a mixed Gaussian-plane-wave representation, we calculated the self-consistent band structures of Mo and W, and compared them with the available augmented-plane-wave results. We find good agreement in the internal structure of the *d* bands, however, the present non-muffin-tin self-consistent calculation yields substantially different *s-d* and *p-d* splittings. The bonding characteristics and Fermi surfaces in these materials are discussed. Finally, we show that these first-principles potentials provide a topological separation of both the octet $A^N B^{8-N}$ and the suboctet $A^N B^{P-N}$ $(3 \leq P \leq 6)$ crystal structures. It is concluded that the presently developed pseudopotentials can be successfully used for studying both the electronic structure of wide range of materials and structural properties, without resorting to empirical parametrization.

I. INTRODUCTION

In a previous paper[1a] (hereafter referred to as I), we have presented a general method for obtaining first-principles atomic nonlocal pseudopotentials in the local-density-functional (LDF) formalism by direct inversion of the corresponding all-electron eigenvalue equations. We have computed these potentials in numerical form for 68 transition and nontransition elements from the first five rows of the Periodic Table and discussed the chemical regularities reflected in their form. We have shown that these potentials accurately reproduce the atomic energy eigenvalues, total energy differences, wave-function moments, and valence charge densities of the underlying all-electron density-functional formalism over a wide range of excitation energies. These potentials contain no empirical data and no adjustable parameters. They are obtained in closed form in terms of the microscopic constructs of the all-electron problem, such as the repulsive Pauli force, orthogonality hole potentials, and valence screening. As such, they should offer greater insight into the reasons for both the successes and the failures of pseudopotential theory in interpreting observed quantities, relative to the empirically adjusted model pseudopotentials.

In the present paper we apply the first-principles pseudopotentials to the study of electronic properties as well as phase stability and structural properties of *solids*. As the valence electronic structure of solids is predominantly sensitive to the low-momentum ($\vec{q} \approx 2\vec{k}_F$, where $\vec{k}_F$ is the Fermi momentum) components of the effective crystal potential whereas the crystal structure and total energies are determined also by the high-momentum potential segments, a combined study of these properties should offer the opportunity to examine the quality of the first-principles pseudopotentials in an extended momentum range.

II. APPLICATIONS TO BAND-STRUCTURE CALCULATIONS

A. Methodologies of construction of first-principles density functional pseudopotentials

The details of our approach for the construction of the density functional nonlocal pseudopotentials are given in I. Here we briefly indicate the underlying methodologies and discuss some of the implications of our approach.

1. Density functional pseudopotential

Let $\{\psi_{nl}^{c,v}(r)\}$ and $\{\epsilon_{nl}^{c,v}\}$ indicate the occupied core (c) and valence (v) wave functions and energy eigenvalues, respectively, obtained from the all-electron (core and valence) density-functional

(DF) equations for an atom in the electronic configuration g. We intend to construct a suitable total energy expression and single-particle eigenvalue problem which applies to the valence subspace alone *and is defined solely by the DF orbital space.*

We first set a DF total energy expression which describes the energy of a fictitious (pseudo) atom having only N_v (valence) electrons with density $n(r)$ and interacting mutually via the interelectronic coulomb $V_{ee}[n(r)]$ and exchange-correlation $V_{xc}[n(r)]$ potentials akin to the DF approach, as well as with a yet unspecified external potential $V_l(r)$. Using a DF variational approach we will derive from this a corresponding single-particle (pseudopotential) equation with eigenvalues $\bar{\epsilon}_{nl}$ and orbitals $\chi_{nl}(r)$. We will impose a number of physically desirable constraints on $\bar{\epsilon}_{nl}$ and $\chi_{nl}(r)$ via a Lagrange-multiplier technique and use them to solve for the unknown pseudopotential $V_l(r)$ which satisfied them.

The constraints are (i) the one-electron spectrum $\bar{\epsilon}_{nl}$ of the pseudopotential problem equals the valence spectrum ϵ^v_{nl} of the all-electron problem, for the chosen reference electronic configuration g; (ii) the pseudo orbitals $\chi_{nl}(r)$ be normalized and nodeless for each of the lowest angular symmetries; (iii) the pseudo orbitals $\chi_{nl}(r)$ be given as a rotation in the all-electron "true" orbital space $\{\psi^{c,v}_{nl}(r)\}$, i.e., $\chi_{nl}(r)=\sum_{n'} C^{(l)}_{n,n'}\psi^{c,v}_{n'l}(r)$. The coefficients $\{C^{(l)}_{n,n'}\}$ are then chosen to minimize the matrix element $\langle\chi_{nl}|\hat{P}_c|\chi_{nl}\rangle$ of the core projection operator $\hat{P}_c$. This leads to a $\chi_{nl}(r)$ which has a minimal amplitude in the core region and maximum similarity, possible within the DF orbital space, to the corresponding "true" valence orbital $\psi^v_{nl}(r)$ in its chemically important "tail" region.

Condition (i) assures that the one-electron spectral properties obtained in the pseudopotential representation match those of the underlying all-electron system. Condition (ii) will allow us (cf. Sec. II C) to expand the pseudo-wave-functions in a simple and spatially smooth basis set, relieving us from the necessity, characteristic of the all-electron approach, to accurately describe the complex and strong spatial variations of the wave functions near the core region which is usually inert to chemically and physically interesting interactions. Condition (iii) establishes a simple unitary relation of $\chi_{nl}(r)$ to the all-electron orbital space, which will allow us, if so desired, to recover the "true" orbital $\psi^v_{nl}(r)$ from the pseudo orbital, simply by core orthogonalization (see Sec. II D and Table II). The maximum similarity constraint of $\chi_{nl}(r)$ to $\psi^v_{nl}(r)$ in the tail region as well as the minimum core amplitude will assure us that the chemical information characteristic of $\psi^v_{nl}(r)$ will be contained in $\chi_{nl}(r)$ and that this will continue to be so, to a good approximation, even if the pseudopotential is to replace the core electrons in chemical environments other than those used to derive it. Stated formally, we are lowering the energy dependence of the pseudopotential by minimizing the orthogonality hole through a core-projection minimization. Physically, we mean that although we derive the pseudopotential from information on a certain atomic electronic state g, this potential will be transferable to within a good approximation to different chemical environments (e.g., excited atoms, molecules, solids, surfaces). This expectation is confirmed by our calculations,[1a] where we find that a DF pseudopotential derived from the atomic ground-state orbitals continues to yield very precise orbital energies (i.e., errors of less than 0.1 eV) when applied to excited configurations over a 25-eV range of excitation energies.

The calculation of any physical observable from $\chi_{nl}(r)$ rather than from the "true" wave function $\psi^v_{nl}(r)$ will inevitably include errors due to the elimination of the nodal structure from $\chi_{nl}(r)$. The corrections to $\chi_{nl}(r)$ are simply described in the present scheme by the core-orthogonality terms $\langle\chi_{nl}|\psi^{\text{core}}\rangle\psi^{\text{core}}$:

$$\chi_{nl}(r)=\sum_{n'} C^{(l)}_{n,n'}\psi^{c,v}_{n'l}(r)\,, \tag{1a}$$

$$\psi^v_{nl}(r)=\frac{1}{C^{(l)}_{n,n}}\left\{\chi_{nl}(r)-\sum_{\text{core}}\langle\chi_{nl}|\psi^{\text{core}}\rangle\psi^{\text{core}}_{(r)}\right\}. \tag{1b}$$

Note that as $\chi_{nl}(r)$ may have different forms in the core region when the atomic core is placed in different chemical environments or electronic states, the error $\Delta=\sum_{\text{core}}\langle\chi|\psi^{\text{core}}\rangle$ is *state dependent.* The pseudopotential derived from $\chi(r)$ is hence energy dependent and may not be transferable from one system to the other. This is treated in the DF pseudopotential approach by directly minimizing Δ via a core-projection-minimization criterion, and at the same time enforcing a maximum similarity constraint of $\chi_{nl}(r)$ to $\psi^v_{nl}(r)$ outside the core region. Note that the extreme limit of this minimization can be achieved by zeroing $\chi_{nl}(r)$ and its first derivatives at the origin, leading naturally to small $\langle\chi|\psi^{\text{core}}\rangle$. Since the leading terms in the pseudopotential are of order $\chi''(r)/\chi(r)$, the choice of a pseudo-wave-function with a limiting behavior of $\lim_{r\to 0}\chi(r)=a_0r^{\lambda+l}+a_1r^{\lambda+l+1}+a_2r^{\lambda+l+2}+\cdots$ for *any* $\lambda\geq 2$ leads to a "hard" pseudopotential with $\lim V_l(r)=\alpha_l r^{-2}$ and $\alpha_l>0$ and an exceedingly small energy dependence. Choosing $\lambda=0$ one obtains a "soft" potential with $\lim V_l(r)=\text{const}$, higher amplitudes of χ_{nl} in the core region, and larger corrections Δ. One can obtain a small core overlap with the choice of $\lambda=0$ if the pseudo-wave-function

is allowed to be nonmonotonic (e.g., a spike at the origin followed by a low amplitude). Such a pseudo-wave-function would, however, require a more extended basis set for its expansion in electronic-structure calculations. A central point in the DF pseudopotential approach is that one can generate continuously "softer" pseudopotentials by the choice of $\{C_{n,n'}^{(l)}\}$, compromising thereby with (i) the range ΔR (between a cutoff point R_c and infinity) at which $\chi_{nl}(r)$ is equal to the "true" wave function and (ii) the energy dependence of the pseudopotentials. Although there exist a parameter range where a reasonable compromise can be achieved between softness and accuracy (see Sec. IIC), we usually prefer the well-defined limit of hard potentials.

Having established a set of physically motivated conditions on $\bar{\epsilon}_{nl}$ and $\chi_{nl}(r)$, we apply a constrained variational treatment to the pseudopotential total-energy expression [1a] and solve for $V_l(r)$ in terms of $\{\epsilon_{nl}^{c,v}, \psi_{nl}^{c,v}$, and $C_{n,n'}^{(l)}\}$. We refer to this as the *density functional pseudopotential* to emphasize that it is constructed from the DF orbital space alone. The closed-form result (Paper I) has a physically transparent form interpretable in terms of an analytical Pauli repulsive term replacing the orthogonality constraint, a screened core potential, an exchange-correlation nonlinearity term, as well as a Coulomb and exchange-correlation orthogonality hole potentials. In I, we have calculated $V_l(r)$ for 68 atoms and demonstrated quantitatively that the desired similarity to the all-electron results (i.e., in the ground-state and excited-state wave functions, orbital energies, and total energy differences) is achieved to within a very good accuracy. Similarly, the low pseudopotential energy dependence and the close simulation of chemical trends across the periodic table are demonstrated. Applications to diatomic molecules, transition metals, and their cohesive properties have similarly shown very good results.

2. *Trans density functional pseudopotential*

The construction of $\chi_{nl}(r)$ in Eq. (1a) from a linear combination of the occupied DF orbital space will always lead to a finite difference between $\chi_{nl}(r)$ and $\psi_{nl}^{v}(r)$ asymptotically as r goes to infinity. As the DF space $\{\psi_{nl}^{c,v}(r)\}$ is orthogonal, the coefficient $|C_{n,n}^{(l)}|^2$ multiplying the $\psi_{nl}^{v}(r)$ in the linear combination is always smaller than unity, leading to $\lim_{r\to\infty}\chi_{nl}(r) = C_{n,n}^{(l)}\psi_{nl}^{v}(r)$ rather than to $\psi_{nl}^{v}(r)$. This is an inevitable consequence of our choice to remain in this unitarily rotated DF space. These large-r discrepancies show up for instance in a deviation of 1%–3% in the pseudo-orbital moment $\langle\chi_{nl}|r|\chi_{nl}\rangle$ from the "true" moment $\langle\psi_{nl}^{v}|r|\psi_{nl}^{v}\rangle$. Although small, such deviations may be noticeable in solid-state applications for crystals with an "open" structure such as Si, where the large-r behavior of the orbitals contributes to the bond charge density. To correct for this small difference, one has to go outside the DF orbital space. We chose to do that in a controlled way by adding to $\chi_{nl}(r)$ an analytic component $f_{nl}(r)$ which will permit $C_{n,n}^{(l)} \equiv 1$. The modified orbital $\hat{\chi}_{nl}(r)$ is

$$\hat{\chi}_{nl}(r) = N\left\{\sum_{n'\neq n} C_{n,n'}^{(l)}\psi_{n'l}^{c,v}(r) + f_{nl}(r)\right\} + \psi_{nl}^{v}(r)\,, \quad (2a)$$

with

$$\psi_{nl}^{v}(r) = \hat{\chi}_{nl}(r) - \sum_{\text{core}}\{\langle\hat{\chi}_{nl}|\psi^{\text{core}}\rangle - N\langle f_{nl}|\psi^{\text{core}}\rangle\}\psi_{(r)}^{\text{core}} - Nf_{nl}(r)\,, \quad (2b)$$

where N is a normalization constant. Any regular function $f_{nl}(r)$ which is nonorthogonal to $\{\psi_{nl}^{c,v}\}$ *and decays rapidly to zero at large* r [so that $\lim_{r\to\infty}\hat{\chi}_{nl}(r) = \psi_{nl}^{v}(r)$] is adequate. We use the simple choice for the cutoff function:

$$f_{nl}(r) = -|A_{nl}|r^{\lambda+l}\exp(-\alpha_{nl}r)\,. \quad (3)$$

The constants A_{nl}, α_{nl} are chosen in an iterative procedure so that conditions (i)–(iii) above remain valid. This leads to a simple quadratic algebraic equation for A_{nl} as a function of α_{nl} whose solution satisfies the normalization of $\hat{\chi}_{nl}$. α_{nl} is then determined by requiring $\hat{\chi}_{nl}(r)$ to remain nodeless and that the pseudo orbital charge accumulation function $Q_{nl}^{\text{PS}}(R) = \int_0^R|\hat{\chi}_{nl}(r)|^2 dr$ match the corresponding all-electron valence orbital accumulation function (starting from $R=\infty$) up to the smallest R value possible under the above constraints. *This leads to* $\hat{\chi}_{nl}(r)$, *which is numerically equal to* $\psi_{nl}^{v}(r)$ *to a point* R_c *inward to the last radial maxima of* $\psi_{nl}^{v}(r)$ and is somewhat more contracted in the core region relative to $\chi_{nl}(r)$. This guarantees that the electrostatic potential outside R_e is identical in the all-electron and the pseudopotential representation.[1b] The orbital moments $\langle\hat{\chi}_{nl}|r^p|\hat{\chi}_{nl}\rangle$ for $p = 1, 2, 3$ are now within less than 1% from the values obtained from $\psi_{nl}^{v}(r)$.

Note that, much like in the DF approach, one can choose in Eq. (3) $\lambda = 2$, obtaining thereby a very low-amplitude pseudo-wave-function in the core region with its associated hard-core pseudopotential and small energy dependence or, conversely, one may choose $\lambda = 0$ and obtain a soft pseudopotential. We find again that a strong pseudopotential produces a larger range ΔR (between R_e and infinity) where $\hat{\chi}_{nl}(r)$ can be made identical to $\psi_{nl}^{v}(r)$, and hence prefer the choice $\lambda = 2$.

The modified pseudo orbital $\hat{\chi}_{nl}(r)$ is used exactly as before[1a,b] to obtain the pseudopotential $V_l(r)$. We refer to this as the *trans density functional* (TDF) pseudopotential to emphasize that an orbital component lying outside the DF space is needed for its

construction. We apply $V_l(r)$ (Fig. 1) for bulk Si in this paper. It seems that the DF pseudopotential, being conceptually and analytically simple, will suffice for most applications. When, however, greater numerical precision is required (e.g., total energy calculations for opened-structure system), the TDF pseudopotential should be preferred. A detailed comparison of the DF and TDF pseudopotentials is given elsewhere.[1b]

Both the DF and TDF pseudopotentials have simple and often desirable analytic properties. In particular, they allow us to recover to within a good approximation the "true" wave functions simply by using Eqs. (1b) or (2b) and the known core orbitals (see Sec. IID). This permits a precise assessment of the accuracy of the calculation of physical quantities from pseudo rather than from "true" wave functions. We note, however, that the performance of a core orthogonalization is merely *an option* afforded by the DF and TDF approaches, and not a *necessity*, as both methods explicitly guarantee a minimal departure of the expectation values of $\hat{\chi}$ from those calculated with ψ^v. Our experience indicates, however, that even if the need for core-orthogonality corrections is minimized to an extreme (possible within the physically motivated constraints imposed), a number of physically interesting properties (e.g., x-ray-structure factors) may be sensitive to such corrections.

The DF and TDF approaches allow for a simple recovery of the true wave functions because of the *linear* relations (1a) and (1b) between the pseudo-wave-functions and a canonical orbital space. If these properties can be sacrificed, yet a third method for constructing first-principles pseudopotentials is possible.

3. *Analytically continued orbital approach*

In this approach one abandons the simple physical description of the pseudo-wave-functions as a linear rotation in a core and valence orbital space, and represents it instead by an arbitrary and numerically convenient functional form. One possibility is to set the pseudo orbital $\tilde{\chi}_{nl}(r)$ to be equal to the valence all-electron orbital $\psi^v_{nl}(r)$ from $r=\infty$ to $r=R_c$ and then analytically continue it to $r=0$ in a smooth form:

$$\tilde{\chi}_{nl}(r)=\begin{cases}\psi^v_{nl}(r); & r>R_c\\ F_{nl}(r); & r\le R_c.\end{cases} \tag{4a}$$

Here $F_{nl}(r)$ can be

$$F_{nl}(r)=\sum_{i=0}^{M} a_{il} r^{\lambda+l+i}, \tag{4b}$$

where λ is a constant. The coefficients a_{il} are determined from continuity requirements $F_{nl}(R_c)=\psi_{nl}(R_c)$; $F'_{nl}(R_c)=\psi'_{nl}(R_c)$; $F''_{nl}(R_c)=\psi''_{nl}(R_c)$; $F'''_{nl}(R_c)=\psi'''_{nl}(R_c)$ as well as from the normalization condition $\int|\tilde{\chi}_{nl}|^2 dr=1$. Such an approach has been recently used by Christiansen *et al.*[1c] in the Hartree-Fock scheme. In the LDF context, we use $M=4$, calculate the derivatives to high numerical accuracy by a Spline scheme, and solve the resulting set of five algebraic equations as a function of R_c. We seek the smallest R_c value for which a nodeless, normalized, and monotonic pseudo orbital $\tilde{\chi}_{nl}(r)$ can be obtained. From this, the pseudopotential is obtained as in the DF and TDF schemes. We refer to this as the *analytically continued* pseudopotential approach. As before, the choice of $\lambda=2$ leads to hard-core potentials while $\lambda=0$ leads to soft-core potentials. The form (4b) is not unique and was chosen since it is the natural description of a central-field atomic orbital at small r and leads to simple analytic forms for the derivatives and the normalization. Exponential forms for $F_{nl}(r)$ are possible as well. Note that the critical feature of $F_{nl}(r)$ which determines the strength of the corresponding pseudopotential is the first power of r which is larger than 1 in its small-r expansion. If this power is 2 the potential is hard $[\lim_{r\to 0}F''(r)/F(r)=\infty]$, while if it is larger than 2 the potential is soft $[\lim_{r\to 0}F''(r)/F(r)=\text{const}]$.

We have applied the analytically continued pseudopotential approach to eight atoms. We find that the resulting potential is numerically identical to the TDF potential from $r=\infty$ to $r=R_c$. The central result is that *the minimum possible value of R_c is pinned to a narrow range near the outer maximum of $\psi^v_{nl}(r)$, much like the R_c value obtained in the TDF approach.* This simply indicates that there exist a fixed nonzero charge $Q^{PS}_{nl}(R_c)\cong Q^{PS}_{nl}(R_e)$ residing in the core region of the pseudo orbital which cannot be eliminated if a normalized, smooth, and nodeless orbital is required. The TDF and the analytically continued orbital approach directly minimize $Q^{PS}_{nl}(R_e)$ and hence achieve the largest spatial range of similarity between the pseudo and true orbitals. The DF approach, restricted to an orthogonal orbital space, typically yield $Q^{PS}_{nl}(R_e)$ values which are 5% larger. Hence, as long as one attains a matching between the true and pseudo-wave-functions asymptotically as r goes to infinity, the *relevant* aspect of the description of $\chi(r)$ at small r is the degree to which a given choice minimizes $Q^{PS}_{nl}(R_c)$. In this respect the hard-core pseudopotential is *unique* in that for *any* $\lambda\ge 2$ the potential starts off at small r as α_l/r^2 and produces a smaller core charge, lower energy dependence, and a larger region ΔR of identity between the pseudo and true wave functions, relative to a soft-core pseudopotential. Due to its small-r form of α_l/r^2, the hard-core pseudopotential will

always have a crossing point r_l (i.e., where the screened pseudopotential crosses the r axis). In Sec. III we show that these quantities form a unique scale reflecting many of the chemical regularities of atoms in the periodic table and, in particular, correlating with the stable crystal structure of compound.

In this paper, we use the TDF pseudopotentials for Si and Ge and the DF potential for the closely packed metallic solids. It will seem that while the TDF and the analytically continued orbital approaches yield numerically accurate pseudopotentials, the basic conceptual framework for constructing nonempirical LDF pseudopotentials is contained already in the DF pseudopotential method. Hence, while different experimentations with the functional choice of $f_{nl}(r)$ [Eq. (2)], $F_{nl}(r)$ [Eq. (4b)], and λ [Eq. (4b)] lead to *families* of pseudopotentials which may be tailored to specific applications or expansion basis sets, the unambiguous DF pseudopotential approach lends itself to a *simple* and physically transparent interpretation and to sufficiently accurate results for most problems.

B. Qualitative comparisons with semiempirical potentials

The first-principles pseudopotentials developed in I have a shape significantly different from that of both the empirical[2] and semiempirical[3] model potentials that have been very successful in describing the band structure of many solids. We discuss here the implications of these differences on the electronic structure of atoms and solids.

Figure 1 depicts the core potentials of Si as obtained in the present first-principles local-density approach[1b] (full lines), the first-principles Hartree-Fock (HF) approach[4] (dashed lines) and the semiempirical model potential method[3] (dot-dashed lines). The latter potential is local and has been designed to fit the overall features of the band structure within a smooth form. It has been used in numerous studies of the bulk, surface,[5] interface,[6] and vacancy problem[7] and is similar in shape to the potential developed by Appelbaum and Hamann[8] for studying surface and chemisorption problems. The HF potential[4] has been previously used for studying various silicon containing molecules and reproduces the all-electron *ab initio* HF results very well. Clearly, the semiempirical potential differs substantially from both the first-principles potentials in the core region (the former lacking turning points) and in the valence region, close to its minima. Since Si lacks an $l=2$ core state, its d potential is purely attractive over all space. These differences in the potentials cannot be dismissed as irrelevant to the valence states of the atom as they have a maximum at the

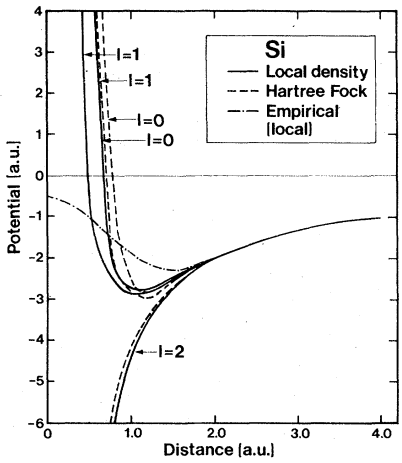

FIG. 1. Core pseudopotentials of Si as obtained in the present first-principles density-functional approach (solid line), the Hartree-Fock approach (Ref. 4) (dashed line), and the semiempirical approach (Ref. 3) (dot-dashed line). The first two potentials are nonlocal while the third is local.

points where the $3s$ and $3p$ pseudo-wave-functions reach values of 65% and 94% of their maxima, respectively. Direct application of the semiempirical potential to the self-consistent calculation of the Si atom indeed reveal discrepancies of 0.60 and 0.70 eV in the $3s$ eigenvalues for the ground and singly ionized configurations, respectively, relative to the "exact" all-electron results obtained by using an identical exchange functional with $\alpha=\frac{2}{3}$. The errors in the orbital moments are 6% and 8%, respectively. Hence, since the semiempirical potential approach attempts to fit the overall band structure with a soft-core or smooth form, deviations for atomic structure relative to "exact" all-electron results exist. The corresponding deviations in the first-principles potentials are smaller by more than an order of magnitude.[1a,b] Similar accuracy is enjoyed by the first-principles HF pseudopotentials.[4,9] The comparison shown here for Si is also characteristic of other atoms (e.g., C, Ge) for which similar semiempirical potentials are available.[10]

Inspection of the orbital kinetic energies of the Si atom discloses part of the reason for the differences in results: the semiempirical potential results in extended wave functions having about 30% less kinetic energy than the corresponding first-principles-derived wave functions. Although this causes significant errors in describing atomiclike configurations, one expects that the differences between these potentials in the valence region would have a smaller effect on the electronic structure of the solid. This stems from the fact that a larger part of the wave function extends towards the bond center, forming a covalent charge buildup and

thereby decreasing the relative importance of the kinetic energy in favor of the more crucial role of the potential energy. As all the potentials shown in Fig. 1 are nearly identical at a distance corresponding to the bond center in bulk Si (2.22 a.u.), one would expect the corresponding valence-band structure to be roughly similar.

One similarly does not expect the significant differences in the potentials near the classical turning points to show up strikingly in the corresponding valence-band structure as the steep portion of the potential is sampled only by high-momentum transfer scattering events which do not affect the dispersion of the bands near $\vec{k}_F$.[11] The success of the "on the Fermi sphere" approximation[12] in describing many of the features of the valence band structure of semiconductors and the sufficiency of the first few reciprocal-lattice-vector Fourier components of the potential to obtain reasonable band structures[12,13] are in line with this notion. Further, when a model potential is constrained to fit only the low-energy interband spectra,[3] inclusion of high-momentum potential components often introduces linear dependence[14] and leads only to nearly rigid ($\vec{k}$-independent) shifts in the positions of the energy bands. One notes, however, that the high-momentum components apparent in the first-principles potential (which are associated with its steep portions near the classical turning points) might be of crucial importance for the study of phase stabilities and lattice vibrations.[15] We will return to this point in Sec. III.

C. Practical considerations

The highly repulsive character of the first-principles pseudopotentials in the region of its classical crossing points (cf. Fig. 1) gives rise to long tails in its Fourier representation. While this poses no practical difficulty when the electronic structure problem is formulated in real space (e.g, using Gaussian[16] or exact numerical atomic orbitals[17] and real-space integration techniques[17,18]), these long tails require a large number of basis functions in reciprocal-space representations.[2,3] Although the recent advent in integration techniques and orbital optimization methods have made the real-space representations of the crystalline wave functions both economic and accurate, the reciprocal-space techniques are computationally simpler. Hence we investigate here possible ways of suppressing the high-momentum components of the pseudopotentials.[19]

We first inquire as to how sensitive the valence electronic structure is to the details of the repulsive part of the potential. We use the behavior of excited atomic species as a probe to the response of the system to modifications in the repulsive potential. We have used various forms of truncating functions (such as Gaussian continuation of the form $Ae^{-\gamma r^2}$, parabolic continuations, and various combinations of hypergeometric functions) that smooth the effective potential with continuous first derivative, requiring that such smoothing leave the energy eigenvalues and orbital moments unchanged to within 1% over a typical excitation energy range of a rydberg. We have found that such smoothing is possible with a wide range of truncating functions *provided the classical crossing points* r_l^0 *and the potential for* $r > r_l^0$ *are untouched.* Some examples are given in Fig. 2 where the original effective potentials of C and Si are compared with the potentials smoothed in the inner core. We find, however, that modifications of the *turning points* lead to rapid deterioration of the quality of the potentials over the entire energy range due to the variational tendency of the charge density to penetrate the core regions where the Coulomb potential is attractive. These small-r smoothing procedures hence offer an approximate but practical way of employing the first-principles potentials in plane-wave representations. Note, however, that the localized nature of these potentials *outside* r_l^0 (e.g., for $l=2$ in transition metals) may still require a large number of plane waves in its reciprocal-space representation and is more naturally described by suitably localized real-space expansions (see below).

A different and equally effective method of suppressing the high-momentum components of the potential is based on overmixing core character into the pseudo-wave-functions.[19,20] If the wave-function transformation coefficients $C_{nl,n'l}$, constructed to lead to a maximum similarity between the nodeless pseudoorbital $\chi_{nl}(r)$ and the true valence orbital $\psi_{nl}(r)$, are artifically scaled to include in $\chi_{nl}(r)$ more core character than needed to satisfy this constraint, $\chi_{nl}(r)$ becomes finite at the origin and the repulsive part of the potential becomes smoother.[20] In the simple case of a first row atom one has

$$\chi_{2s}(r) = C^0_{2s,1s}\,\psi_{1s}(r) + C^0_{2s,2s}\,\psi_{2s}(r), \tag{1c}$$

where $C^0_{2s,1s}$ and $C^0_{2s,2s}$ are determined such that $\chi_{2s}(r)$ be nodeless and smooth (i.e., satisfy minimum kinetic energy) and possess the maximum similarity to $\psi_{2s}(r)$ possible under these constraints. This leads to $\chi_{2s}(0)=0$ and a repulsive potential. As $C^0_{2s,1s}$ is replaced by $C^0_{2s,1s}+\delta$ one obtains $|\chi_{2s}(0)|>0$ and a resulting smoother potential. This is illustrated in Fig. 3 where the $l=0$ component of the screened carbon core potential is displayed for various choices of δ. As core character is overmixed, the node q_0 in $V_{\rm eff}(q)$ moves outwards

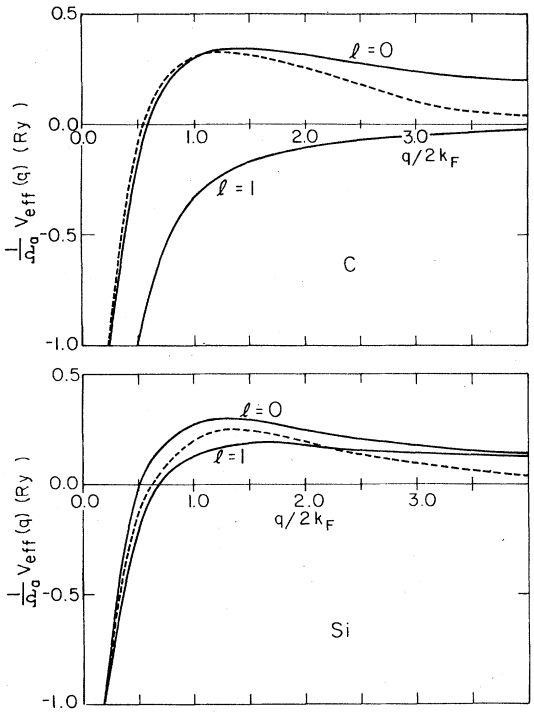

FIG. 2. Screened core pseudopotentials of carbon and silicon as obtained from the maximum similarity first-principles approach (solid lines), compared with the $l=0$ potentials smoothed in the inner core (dashed lines). The unit cell volume and the Fermi momentum are denoted by Ω_a and k_F, respectively.

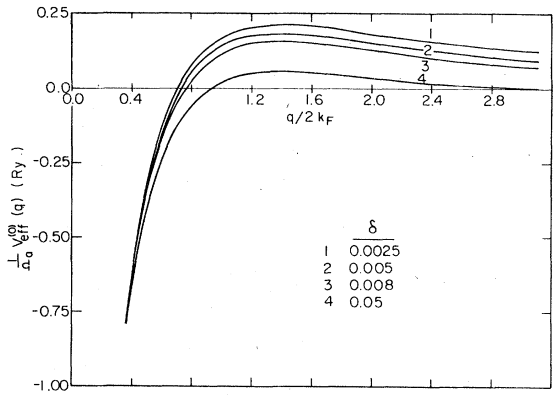

FIG. 3. $l=0$ component of the screened carbon pseudopotential, as obtained by various degrees of core overmixing δ into the $2s$ pseudo-orbital.

and the potential is suppressed at large momenta. These changes clearly illustrate the relationship between the potential truncation at large q and the variational quality of the resulting wave functions: as more of the core orbitals are admixed into a given valence pseudoorbital, its similarity to the all-electron valence wave function deteriorates while the high-momentum components of the potentials are reduced due to the decreased repulsiveness of the Pauli potential. *One can hence obtain almost an arbitrarily short-range potential in momentum space at the expense of the quality of the valence wave functions.* The examples given in Fig. 3 represent the range of changes in which a reasonable compromise between the accuracy of the wave functions and the range of the potential can be achieved. We stress, however, that these smoothing procedures are motivated solely by computational considerations associated with the use of "conventional" plane-wave expansions and can be largely circumvented as more flexible expansion methods are employed (see below).

As a test for the performance of the first-principles pseudopotentials in describing the electronic structure of solids we have performed self-consistent band calculations for a "representative" semiconductor (Si and Ge) and transition metals (Mo,[21] W). Applications to electronic properties of diatomic molecules (e.g., O_2, Si_2) will be presented elsewhere. As the aim of this study was to obtain close predictions of the currently developed potentials rather than to provide economic forms of the potentials, we have smoothed the effective potentials only very close to the nucleus ($r \leq 0.2$ a.u.) to maintain the numerical stability of the currently employed expansion technique. The resulting atomic wave functions and energies are unchanged relative to the unsmoothed potential by 10^{-2}% and 0.01 eV, respectively.

We have used two methods for self-consistently solving the nonlocal band problem: The plane-wave[2,3] and the mixed-basis[22] methods. As these methods are well known, we will only mention briefly the pertinent details for the present study.

The plane-wave method (e.g., Ref. 3) uses a reciprocal-space Fourier expansion of the core pseudopotential and the valence (screening) potential. The relevant expansion coefficients are computed by radial numerical integration. We retain the $l=0$, 1, and 2 components of the potential as the $l>2$ character of the wave functions is presumably small in the energy range of interest. The potential is used directly in a numerical form, without fitting it to analytic equations. The only convergence problem in this scheme is associated with the number of plane waves retained in the wave-function and potential expansion. We have performed convergence tests to obtain an accuracy of 0.1 eV or better in the energy eigenvalues. The number of waves required for this accuracy is ~280 for Si and Ge plus an additional 255 waves in a second-order Löwdin perturbation expansion[23] and ~480 for the transition metals, with additional 225 waves in a second-order expansion.

As this approach is costly due to the large number of plane waves required, it was used primarily to obtain a standard for converged results. The mixed-basis approach offers much improved convergence as the localized features of the wave functions are represented by suitably peaked Gaussians basis function while the remainder of the wave functions is expanded in plane waves. The Gaussian exponents are varied to obtain rapid convergence in the plane-wave expansion. We obtain an accuracy of better than 0.1 eV in the energy eigenvalues for W and Mo by using d Gaussian exponents of 1.35 and 1.85, respectively, and 95 and 103 plane waves plus five Gaussians per atom, respectively. For Si, a s,p exponent of 1.50 a.u.$^{-2}$ was found to be optimal. The mixed-basis representation is well suited for the pseudopotentials at hand, and since only valence states are treated (e.g., six electrons for W and Mo), it constitutes a substantial simplification over the all-electron approach to these materials (involving 42 and 74 electrons for Mo and W, respectively).

The calculations are carried to self-consistency in a standard fashion,[3] avoiding muffin-tin or other shape approximations to the potential. The charge density is sampled at six special $\vec{k}$ points in the Brillouin zone (Γ, X, L, Δ, Σ, and W) for the semiconductors and 14 $\vec{k}$ points for the metals. For the latter we compute the density of states, Fermi energy, and the wave-vector- and band-dependent weights at each iteration using the tetrahedron integration scheme.[24] More details about the method and its application to bulk Mo will be given in a different publication.[21]

D. Si and Ge pseudopotential band structure and charge density

The self-consistent nonlocal pseudopotential band structure of Si is given in Fig. 4. We have used the standard Kohn and Sham[25] exchange coefficient of $\alpha = \frac{2}{3}$ and included the homogeneous electron correlation functional of Singwi *et al.*[26] The energy eigenvalues at high-symmetry points are given in Table I where they are compared with the first-principles self-consistent orthogonalized-plane-waves (SCOPW) results of Stukel *et al.*,[27] for $\alpha = \frac{2}{3}$ the semiempirical self-consistent local pseudopotential[28] (SESCL), the empirical non-self-consistent nonlocal (ENSCNL) pseudopotential[29] and with the observed photoemission[30-32] and optical[33] data. Of the four calculations compared, only the ENSCNL[29] is not self-consistent as the effective potential in this approach has a parametric form adjusted to reproduce the bulk interband transitions and photoemission data and is not expressible in terms of the charge density. It has also been shown[29] to give excellent agreement with the cyclotron masses in Si and the shape of the valence charge density. Since it attempts to mimic the *screened* potential in the bulk, it does not provide a mechanism for charge redistribution and cannot be used for Si-containing systems other than bulk Si (e.g., molecules, surfaces, etc.). The semiempirical pseudopotential SESCL has been used with slight modifications in the past for studies on the Si_2 molecule,[34] silicon surfaces,[5] interfaces,[6] and vacancies.[7]

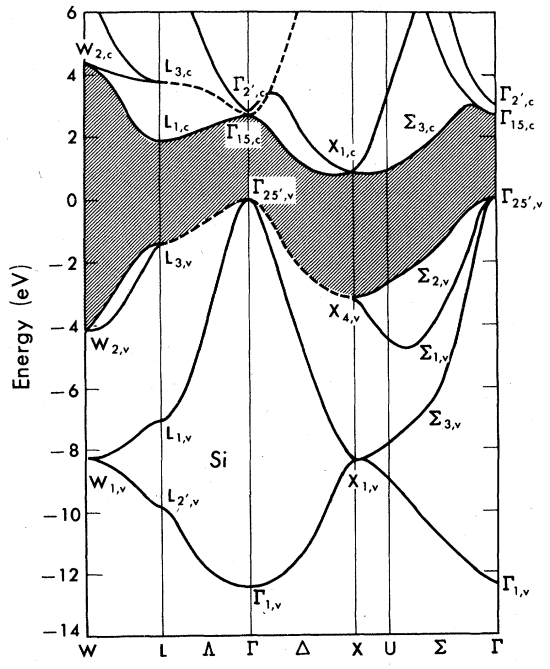

FIG. 4. Self-consistent exchange and correlation band structure of Si using the first-principles nonlocal pseudopotential.

Our results agree well with the experimental data for the occupied states and are in moderately good agreement with the first-principles SCOPW results. The indirect $\Gamma_{25,v}$-$\Delta_{1,c}$ band gap (0.5 eV) is, however, substantially smaller than the observed value of 1.13 eV. Although the agreement between the calculated gap and experiment can be improved by treating the exchange coefficient as an adjustable parameter,[27] this approach will be avoided here. In general, the first-principles results are as good as the empirically adjusted results for the ground occupied states but are systematically lower than both the empirical and the experimental results for the excited states (e.g., discrepancies of 1.65, 0.35, 0.61, and 0.54 eV for the $\Gamma_{2',c}$, $\Gamma_{1,c}$, $X_{1,c}$, and L_{3c} states, respectively). We will discuss this effect later on. As expected, the difference between the results of the local pseudopotential (SESCL) and the present nonlocal pseudopotential are somewhat smaller than the corres-

TABLE I. Comparison of the Si-band eigenvalues (in eV) of the present pseudopotential exchange and correlation study (using a mixed-basis) with the SCOPW (Ref. 27) results ($\alpha=\frac{2}{3}$), the semiempirical self-consistent local pseudopotential ($\alpha=\frac{2}{3}$) (Ref. 28), the empirical non-self-consistent non-local (Ref. 29) and experiment (Refs. 30-33).

Level	SCOPW	Present results	SESCL	ENSCNL	Experimental
$\Gamma_{1,v}$	−12.04	−12.20	−12.82	−12.36	−12.4 ± 0.6 [a]
$\Gamma_{25,v}$	0.00	0.00	0.00	0.00	···
$\Gamma_{2',c}$	3.31	2.50	3.38	4.10	4.15 ± 0.05 [b]
$\Gamma_{15,c}$	2.33	2.48	2.70	3.42	···
$\Gamma_{1,c}$	···	7.25	5.95	7.69	~7.6 [b]
$X_{1,v}$	−7.83	−8.02	−8.51	−7.69	
$X_{4,v}$	−3.00	−2.93	−3.24	−2.86	−2.9 [b], −2.5 ± 0.3 [c]
$X_{1,c}$	0.34	0.52	0.51	1.17	1.13 [d]
$X_{4,c}$	9.87	9.97	11.62	···	
$L_{2',v}$	−9.63	−9.92	−10.41	−9.55	−9.3 ± 0.4 [c]
$L_{1,v}$	−7.14	−7.21	−7.62	−6.96	−6.4 ± 0.4 [a], −6.8 ± 0.2 [c]
$L_{3',v}$	−1.26	−1.28	−1.39	−1.23	−1.2 ± 0.2 [b]
$L_{1,c}$	1.39	1.13	1.45	2.23	
$L_{3,c}$	3.12	3.36	3.48	4.34	3.9 ± 0.1 [b]
$\Sigma_{1,\min}$	−3.95	−4.72	−4.20	−4.47	−4.7 ± 0.3 [a,c]

[a] Reference 31.
[b] Reference 30.
[c] Reference 32.
[d] Reference 33.

ponding differences in the free atom. Note, however, that the semiempirically adjusted SESCL potential yields somewhat poorer agreement with the observed valence-band states, as compared with the first-principles pseudopotential.

As the first-principles core pseudopotential is given as an infinite series of angular momenta components[1] $\sum_{l=0}^{\infty} W_l(\vec{r})\hat{P}_l$ (where $\hat{P}_l$ is the projection operator) and as $W_l(\vec{r})$ for the symmetries which are absent in the core of the free atom is singular (e.g., $l \geq 2$ in Si, cf. Fig. 1) it is important to assess the validity of the truncation of this series. One expects that only those angular-momentum components which are present in the crystalline wave function in an energy range of interest would be important. As the atomic central-field symmetry is removed in the solid, states including $l \geq 2$ components can be admixed into the occupied variational crystal wave functions. We have repeated a self-consistent band-structure calculation for Si, retaining this time only the $l=0,1$ pseudopotential components. We find rather small changes in the valence band spectra (e.g., $L_{1,v}$, $X_{1,v}$, $X_{4,v}$) along with more significant changes (0.3–0.8 eV) in some conduction band states (e.g., $L_{3,c}$, $L_{1,c}$, $\Gamma_{12,c}$ and the Σ_c line). It would hence seem that the higher $l>2$ corrections are unimportant for the energy region below ~5 eV above the conduction-band edge. As one moves down the Periodic Table, one expects, however, the $l \geq 2$ components to become more important (i.e., As, Se) as the d states tend to be bound even in the free

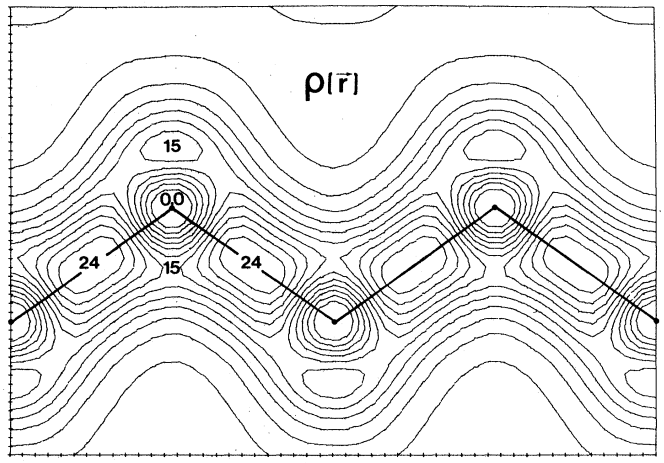

FIG. 5. Total valence pseudocharge density in the (110) plane in Si, as calculated by the present exchange and correlation nonlocal pseudopotential. The full dots indicate the atomic positions. The results are given in units of electron/(crystallographic cell).

atom.

The total valence pseudo-charge-density of Si in the (110) plane is depicted in Fig. 5. The valence charge density obtained from the present first-principles potential differs from that obtained with the SESCL potential in a few respects: The calculation depicted in Fig. 5 yields a bond charge density which is elongated parallel to the bond axis and decays rather steeply towards the atomic site, whereas the semiempirical potential yields a bond charge that is oblate and decays rather slowly towards the atomic site. If one is arbitrarily to define the covalent bond charge density as that enclosed by the outermost contour surrounding the bond, the present calculation yields an anisotropy factor L_1/L_2 (where L_1 is the length of the bond charge parallel to the bond axis and L_2 is the length perpendicular to this axis) of ~1.3 while the SESCL potential yields $L_1/L_2 = 0.8$ and the observed bond anisotropy ratio[35] is about 1.4. The highest value of the valence charge density obtained in this work is 24.0 e/cell while that obtained with the semiempirical potential is 24.2 e/cell and the observed maxima is 23.3 e/cell.[35] We note, however, that the experimentally synthesized valence charge density is not strictly comparable to pseudopotential calculations as (i) the core density is simply *subtracted* in the former case from the total density whereas in a pseudopotential methods the core density is *projected* out (i.e., the valence wave functions are deorthogonalized to the core, leaving a smooth wave function), and (ii) the core density is represented in the experimentally synthesized density by HF (rather than the density functional) orbitals. These are usually more contracted than the local density orbitals.[36] Note that the local pseudopotential gives rise to a single charge density maxima or to closely spaced double maxima in the occupied π_u orbital of the diatomic Si_2 molecule,[34] whereas first-principles LDF[37] calculations and the present[38] pseudopotential predict a well-separated double maxima in either side of the interatomic axis.

Figures 6 and 7 show the valence pseudocharge density of Si at few high-symmetry points in the zone. Both s-type (e.g., $\Gamma_{1,v}$, $X_{1,v}$) and p-type (e.g., $\Gamma_{25,v}$, $X_{4,v}$) states show a distinct charge polarization along the bond axis, suggesting that it is not the potential nonlocality that is responsible for the formation of a bond-polarized charge ($L_1/L_2 > 1$). A local approximation to our potential (i.e., neglecting the $l > 0$ components of the potential) produces indeed $L_1/L_2 = 1.2$. In contrast, we find that the SESCL pseudopotential produces $L_1/L_2 < 1$ for both the s- and the p-type states. The polarization of the bond charge density along the bond direction is a consequence of the more localized nature of the first principles potential (cf. Fig. 1). It is important to note that the differences in the details of the valence charge polarization between the first principles and the semiempirical pseudopotentials do not manifest themselves significantly either in the valence band structure nor in the low-angle forbidden x-ray scattering factor (the [222] reflection being 0.19 e/cell in the present calculation and 0.25 e/cell with the semiempirical pseudopotential). It would seem that only the higher-momentum components ($\vec{q} \gg 2\vec{k}_F$) of the first-principles pseudopotential determine the details of the anisotropy of the charge density. These might be important in determining the total energy, phonon spectra, or chemical reactivity but are hardly material for the one-electron observables related to low-momentum scattering events.

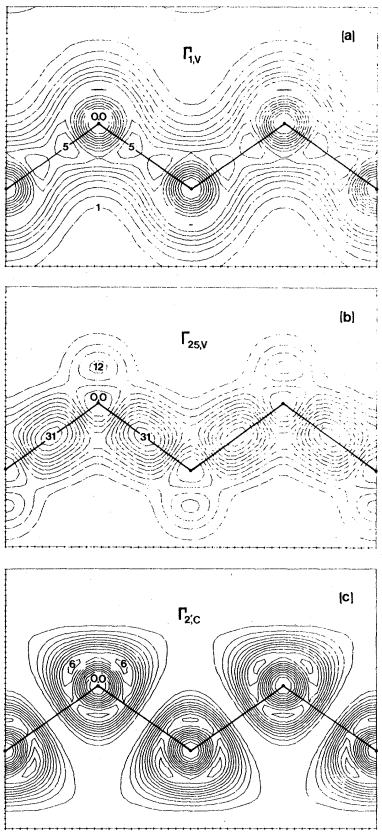

FIG. 6. Symmetrized pseudo charge density in the (110) plane of Si at the Γ point in the zone, as obtained by the present exchange and correlation first-principles (nonlocal) pseudopotential. Full dots indicate the atomic positions. (a) The bonding $3s$-type $\Gamma_{1,v}$ state, (b) the bonding $3p$-type triply degenerate $\Gamma_{25,v}$ state, (c) the antibonding $3s^*$-type $\Gamma_{2',c}$ state.

It is interesting to note in passing that the charge densities of the top and bottom valence bands in Si change very little across the Brillouin zone (e.g.,

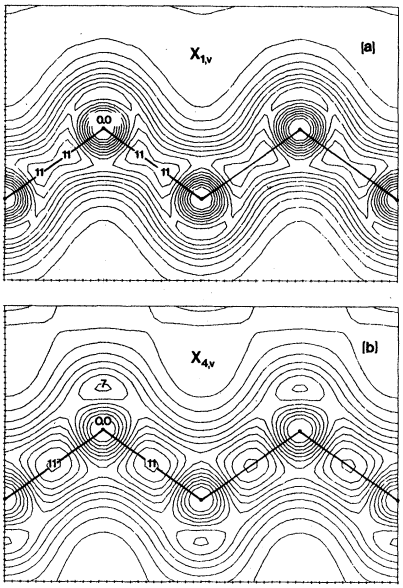

FIG. 7. Symmetrized pseudocharge density in the (110) plane of Si at the X point in the zone, as obtained by the present exchange and correlation first-principles (nonlocal) pseudopotential. Full dots indicate the atomic positions. (a) The bonding $3s$-type $X_{1,v}$ state. (b) The bonding $3p$-type $X_{4,v}$ state.

Γ_{1v}-X_{1v}, $\Gamma_{25',v}$-$X_{4,v}$). The low dispersion of the band density implies that Brillouin-zone sampling techniques based on few representative points[39] are accurate for such systems.

Inspection of the charge density of the highest occupied p-type valence band (e.g., $\Gamma_{25',v}$) and the lowest s-type conduction band (e.g., $\Gamma_{2',c}$, $L_{1,c}$) suggests a reason for the remarkable sensitivity of the p-s gap (e.g., $\Gamma_{25',v}$-$X_{1,c}$, $\Gamma_{25',v}$-$\Gamma_{2',c}$) to scaling of the exchange potential.[27] As the $L_{1,c}$-$\Gamma_{2',c}$ states are strongly antibonding states having a density which is appreciably localized near the atomic sites [cf. Fig. 6(c)], they are particularly sensitive to the enhancement of the exchange potential $\alpha\rho^{1/3}(r)$ (via increasing the exchange coefficient α). On the other hand, the $\Gamma_{25',v}$ valence band is a delocalized $3p$ state [cf. Fig. 6(b)] occupying regions of low charge density and is consequently significantly less sensitive to exchange scaling. The differences in the degree of localization of these states leads to marked changes in the calculated band gaps as the exchange coefficient is increased from $\alpha=\frac{2}{3}$.[27] One further notes that the localized nature of the lowest s-type conduction band in Si might induce important self-interaction effects which are spuriously included in the density functional potential.[40,41] These arise from the imperfect balance between the electronic self-Coulomb and self-exchange interactions and have an appreciable magnitude for localized states both in atoms and solids.[40,42] These usually produce anomalously small band gaps relative both to the self-interaction-compensated calculations[41] and experiment. Hence, although the difference in the degrees of spatial localization of the valence and conduction bands in Si enables the adjustment of the band gap via exchange scaling, the calculated anomalously small band gap appears to have a different and physically distinct origin. As the self-interaction corrections vanish at the limit of extended delocalized states, the high plane-wave-like states of Si are likely to be correctly described by the density functional approach. A direct approach to the self-interaction corrections in the spectra of solids has been previously developed[41]; however, a similar application to Si is outside the scope of the present paper.

Another measure of the quality of the calculated charge density is furnished by comparison with the observed x-ray scattering factors. As the pseudopotential calculation produces nodeless valence wave functions, it is not clear whether these are sufficiently accurate for comparison with the all-electron charge density or with experiment even in the valence region.[29,43] Since our pseudopotential formalism represents the pseudo-wave-functions in the atomic limit as linear combination of the true all-electron core and valence wave functions,[1a,b] it is possible to recover the nodal valence orbitals to within a good approximation by performing an appropriate core orthogonalization.[1,43] The effects of such an orthogonalization in the atomic limit are demonstrated in Fig. 8. Here we plot the difference $\Delta F_1(q)$ between the all-electron *atomic* scattering factor $\int\rho_{c+v}(\vec{r})e^{i\vec{q}\cdot\vec{r}}\,d\vec{r}$ and that computed from the valence pseudodensity $n(\vec{r})$ plus the core density $\rho_c(\vec{r})$: $\int[n(\vec{r})+\rho_c(\vec{r})]e^{i\vec{q}\cdot\vec{r}}\,d\vec{r}$. Here $\rho_{c+v}(\vec{r})$ is constructed from the nodal core (c) and valence (v) orbitals. As both $\rho_{c+v}(\vec{r})$ and $n(\vec{r})+\rho_c(\vec{r})$ are normalized to the total number of electrons in the system, $\Delta F_1(0)=0$ and similarly $\Delta F_1(\infty)=0$ as the high-momentum components sample only the core density $\rho_c(\vec{r})$. At intermediate momentum values, the error $\Delta F_1(q)$ (solid line in Fig. 8) is seen to be non-negligible relative to the experimental errors in determining the scattering factors of bulk[44] Si (vertical bars in Fig. 8 appearing at the first few reciprocal-lattice vectors of Si). Clearly, a direct use of the pseudocharge density instead of the core-orthogonalized density produces some errors even at low momenta. The curve marked $\Delta F_2(q)$ denotes the similar differences produced by the local semiempirical pseudopotential.[3] These are larger by about a factor of 3 and localized in the region where the physically interesting [111] reflection occurs. Upon core-orthogonalizing the first-prin-

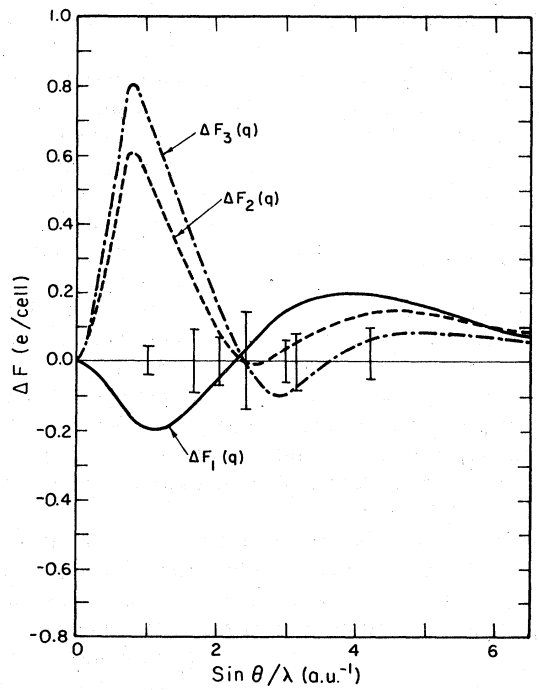

FIG. 8. Differences between the all-electron and the pseudopotential atomic x-ray scattering factors for Si. $\Delta F_1(q)$ denotes the difference obtained with the first-principles pseudopotential; $\Delta F_2(q)$ denotes similar differences obtained with the semiempirical pseudopotential;[3] $\Delta F_3(q)$ denotes the difference obtained when the semi-empirical pseudo-orbitals are orthogonalized to the core orbitals. The corresponding difference with the first-principles-derived orbitals is identically zero. The vertical bars on the abscissa indicate the experimental errors associated with measuring the crystalline scattering factors at the first few reciprocal-lattice vectors (Ref. 44).

ciples pseudo-wave-functions, $\Delta F_1(q)$ for the atom vanishes identically.[1a,b] The corresponding differences in the bulk are not expected to vanish identically as the orthogonalization is performed with respect to the atomic frozen-core orbitals (rather than the variational bulk core wave functions); however, based on our experience with core orthogonalizations of excited state atomic wave functions,[1a,b] we expect to obtain accurate results for the bulk. It is interesting to note that core orthogonalization of the pseudo-wave-functions derived from the semiempirical pseudopotential method[3] (in which the pseudo-wave-functions are not representable as combinations of the true orbitals), produces even larger differences [curve marked $\Delta F_3(q)$] relative to the unorthogonalized results.

Table II shows the calculated x-ray scattering factors in bulk Si obtained by core orthogonalization of the pseudo-wave-functions.[1,43] The orthogonalization has been performed using a three-dimensional Diophantine integration method.[45] The results are compared with the all-electron SCOPW calculation of Stukel *et al.*[27] and with experiment,[44] corrected for the Debye-Waller factor and anomalous dispersion.[27] The present results agree very well with the observed data, and even the sensitive features such as the "forbidden" [222] reflection and the order of the [333] and [555] reflections (degenerate in the atomic superposition limit) are correctly reproduced. Our scattering factors are significantly larger than the SCOPW and the atomic superposition results[27] at low momentum, indicating a more localized valence density in the present calculation. At high momentum, our results are slightly lower than the SCOPW results, possibly due to the use of somewhat different core orbitals in the present scheme which involve homogeneous correlation terms in the potential. The excellent agreement obtained here between the calculated and the observed x-ray scattering factors suggests that the differences between our real-space charge

TABLE II. Comparison of the observed (Ref. 44) and calculated x-ray structure factors for Si (in units of electrons per crystallographic cell). The SCOPW results (Ref. 27) are given for the Kohn and Sham exchange. The present results include free-electron correlation corrections.

	Experimental		Present	Atomic	
[*hkl*]	Ref. 44*b*	Ref. 44*a*	results	superposition	SCOPW
111	10.70	11.12	10.70	10.52	10.69
220	8.48	8.78	8.57	8.70	8.64
311	7.77	8.05	7.79	8.15	8.01
222	0.17	0.22	0.19	0.0	0.17
400	7.08	7.40	7.35	7.47	7.44
331	6.81	7.32	7.03	7.14	7.21
422	6.21	6.72	6.65	6.65	6.68
333	5.87	6.43	6.31	6.39	6.38
511	5.88	6.40	6.35	6.39	6.42
440	7.65	6.04	6.00	6.03	6.02

TABLE III. Calculated Fourier coefficients of the self-consistent Coulomb screening [$V_{\text{Coul}}(\vec{G})$], exchange screening [$V_x(\vec{G})$], and correlation screening [$V_{\text{corr}}(\vec{G})$] for Si. Results are in rydberg per unit cell volume. $\rho(0)$ is normalized to 8.0 electrons and h,k,l denote the index of plane waves representative of the corresponding stars.

hkl	$V_{\text{Coul}}(\vec{G})$	$V_x(\vec{G})$	$V_{\text{corr}}(\vec{G})$
111	−0.150 64	0.050 76	0.003 76
211	−0.001 54	0.007 22	0.000 79
221	0.008 13	0.007 26	0.000 44
222	0.008 05	0.002 99	0.000 03
220	0.006 25	0.006 92	0.000 43
311	0.001 24	0.002 79	0.000 18
332	−0.001 76	0.003 47	0.000 25
331	−0.001 24	0.002 36	0.000 17
422	−0.000 92	0.001 89	0.000 14
421	−0.000 55	0.002 12	0.000 18
411	−0.000 31	0.000 13	0.000 11
431	−0.000 08	0.000 24	0.000 01
443	0.000 21	0.001 23	0.000 12
442	−0.000 09	0.000 60	0.000 07

density (computed from the lowest 830 scattering factors) and the experimentally synthesized density[35] (obtained by inverting the Fourier series of the lowest 21 observed scattering factors) might originate from limitations of the inversion procedure.[35]

Table III depicts the first few Fourier components of the self-consistent screening field. In each case we give the transform with respect to a single plane wave (with index h, k, l) representative of the corresponding star of $\vec{G}$. A few conclusions pertaining to the screening mechanism in Si emerge from these results. With the exception of the group of 12 reflections belonging to the [211] star, both the exchange (V_x) and the correlation (V_{corr}) fields act to screen the electron-electron Coulomb (V_{Coul}) interactions (i.e., they have an opposite sign). This screening is very effective at short wavelength where $|V_x(\vec{G})/V_{\text{Coul}}(\vec{G})|$ is larger than unity. The Fourier components of the screening potential are divided into a few groups with decreasing importance: the first contains the strongest [111] component (eight members), the second contains the smaller ($V_{\text{Coul}} \sim 0.005$ Ry) components (four stars with a total of 56 members), and finally one finds the higher components having lower contributions ($V_{\text{Coul}} \sim 10^{-9}$–$10^{-5}$ Ry). The band structure appears to be sensitive to variations of the first two groups of components while changes in the high-momentum contributions affect only the details of the charge density (e.g., bond anisotropy). We similarly find that the correlation screening constitutes only about 5% of the exchange screening and decay very rapidly at high momenta. Note that the ratio $V_{\text{corr}}(\vec{G})/V_x(\vec{G})$ varies considerably with $\vec{G}$ for the first two groups of waves and settles to about ~0.05 for the high-momentum parts. This suggest that one cannot simulate these correlation terms effectively for the important low-momentum components by simply linear scaling of V_x. For higher components, an exchange coefficient of 0.70 (instead of the Kohn and Sham value of $\frac{2}{3}$) seems to mimic the combined effects of exchange and correlation reasonably well.

We have performed an analogous study of the band structure and charge density on Ge, using our first-principles pseudopotentials. As the charge density and the corresponding conclusions born out from the study on Si are qualitatively similar, we present only a brief discussion of the resulting band structure. Table IV depicts the calculated band structure of Ge at high-symmetry points, as compared with the SCOPW results of Herman *et al.*[46] and the empricial pseudopotential of Chelikowsky and Cohen.[47]

The agreement between the present first-principles calculation and the empirically adjusted pseudopotential[47] and the SCOPW[46] calculation is very good for all except the low-lying antibonding $4s$ band ($\Gamma_{2',c}$-$X_{1,c}$-$L_{1,c}$) where the present study reveals systematically lower results. The same effect occurs in our calculation on Si and was discussed above. Anomalously low $\Gamma_{25,v}$-$\Gamma_{2',c}$ and $\Gamma_{25,v}$-$X_{1,c}$ gaps have been previously obtained in first-principles OPW studies[48] where it was found that slight empirical adjustments of the calculated Fourier components of the potential are required to bring these results into agreement with experiment. Our calculated valence charge density for Ge is qualitatively very similar to that of Si. The

TABLE IV. Comparison of the present exchange and correlation band structure of Ge with the SCOPW (Ref. 46) and empirical (non-self-consistent) pseudopotential calculations (Ref. 47). Results are given in eV.

	Present results	SCOPW	Empirical pseudopotential
$\Gamma_{1,v}$	−12.36	−12.2	−12.66
$\Gamma_{25,v}$	0.00	0.0	0.00
$\Gamma_{2',c}$	0.77	1.1	0.9
$\Gamma_{15,c}$	2.59	3.0	3.1
$X_{1,v}$	−8.40	−8.4	−8.65
$X_{4,v}$	−2.85	−2.8	−3.29
$X_{1,c}$	0.95	1.3	1.16
$X_{3,c}$	8.92	10.2	···
$L_{2',v}$	−10.09	−10.1	−10.39
$L_{1,v}$	−7.24	−7.1	−7.61
$L_{3',v}$	−1.28	−1.2	−1.53
$L_{1,c}$	0.65	0.9	0.76
$L_{3,c}$	3.95	4.2	4.20
$L_{2',c}$	7.60	7.8	···

bond anisotropy factor L_1/L_2 decreases from the value of 1.3 in Si to 1.1, indicating an increased tendency to form a metallic bond. A local (self-consistent) semiempirical Ge pseudopotential produces a consistently lower bond anisotropy ($L_1/L_2 = 1.0$).

E. Applications to transition metals

As a further test to the quality and generality of the first-principles pseudopotentials we have applied them to study the electronic structure of two transition metals— molybdenum and tungsten. The detailed description of the molybdenum results will be presented elsewhere,[21] and we concentrate here on the tungsten results.

The application of pseudopotential formalism to the study of the electronic structure of transition metals is difficult. This is mainly due to the ineffectiveness of simple plane-wave expansion techniques to describe localized d states, the pronounced nonlocality of transition-metal pseudopotentials[1a] and the lack of sufficient experimental data to parametrize either the single valence-electron–ionic term values or the low-energy interband spectra. The present approach circumvents these difficulties by using a flexible mixed-basis representation[22] capable of treating nonlocal potentials and accurately describing both the localized features of the d states and the extended character of the s-p states. Further, no use is made of experimental fitting techniques in the present first-principles approach.

The establishment of the self-consistency of the crystal potential poses special problems in metals. Whereas in semiconductors and insulators one can approximate the variational crystal charge density by sampling the square of the symmetrized wave functions at few representative points $\vec{k}_i$ in the Brillouin zone (BZ) using equal weights for all the occupied bands at a given point $\vec{k}_i$,[39] the occurrence of a Fermi surface in a metal requires explicit consideration of both wavevector and *band dependent* weights $W_j(\vec{k}_i)$. This results from the fact that the BZ occupation volume depends on the details of the crossing of the Fermi surface by a given band. We treat this problem by sampling a grid of equally spaced inequivalent $\vec{k}$ points in the irreducible zone and computing at each iteration step the density of states (using the tetrahedron interpolation scheme[24]), the Fermi energy, and the fractional volume of each minitetrahedron that lies under the Fermi surface at each band. These band-dependent weights vary at each iteration step with the shape of the Fermi surface. They reflect both the geometric factor associated with each $\vec{k}_i$ point (i.e., nearest BZ volume occupied by $\vec{k}_i$) and an additional factor, absent for nonmetals [in which $W_j(\vec{k}_i)$ reduces to $W(\vec{k}_i)$] which measures the occupancy of volume under the Fermi surface. The sampling weights obtained for 14 principal $\vec{k}_i$ points in tungsten at the self-consistency limit are depicted in Table V.

It is seen that $W_j(\vec{k})$ is band independent for the lowest two valence bands (which are removed from the Fermi surface) and is a decreasing function of the band index for the higher bands which cross the Fermi surface. The weights of the two lowest bands increase initially as one moves away from the Γ points towards H, N, or P due to the increased fractional BZ volume associated with the latter points, while the variation of the weights of the highest bands with wavevector also reflect the vicinity of the band to a Fermi surface area.

TABLE V. 14-k-point band and wave-vector-dependent weights $W_j(\vec{k})$ for the self-consistent tungsten band structure. Weights are normalized to the number of valence electrons per cell (6.0). All weights for $j > 4$ are zero.

$\vec{k}$ point	$W_1(k)$	$W_2(k)$	$W_3(k)$	$W_4(k)$
1 (0.0, 0.0, 0.0)	0.031 25	0.031 25	0.031 25	0.015 073 7
2 (0.25, 0.0, 0.0)	0.125 00	0.125 00	0.125 00	0.032 425 5
3 (0.25, 0.25, 0.0)	0.125 00	0.125 00	0.120 291	0.017 817 6
4 (0.25, 0.25, 0.25)	0.187 50	0.187 50	0.187 50	0.020 074 3
5 (0.50, 0.0, 0.0)	0.125 00	0.125 00	0.120 200	0.018 401 2
6 (0.50, 0.25, 0.0)	0.250 00	0.250 00	0.241 079	0.020 348 4
7 (0.50, 0.25, 0.25)	0.312 50	0.312 50	0.302 910	0.019 202 2
8 (0.50, 0.50, 0.0)	0.093 75	0.093 75	0.079 455	0.000
9 (0.50, 0.50, 0.25)	0.218 75	0.218 75	0.208 670	0.000
10 (0.50, 0.50, 0.50)	0.062 50	0.062 50	0.062 500	0.000
11 (0.75, 0.0, 0.0)	0.062 50	0.062 50	0.038 319	0.001 461 2
12 (0.75, 0.25, 0.0)	0.218 75	0.218 75	0.184 978	0.006 050 6
13 (0.75, 0.25, 0.25)	0.156 25	0.156 25	0.132 069	0.003 053 9
14 (1.0, 0.0, 0.0)	0.031 25	0.031 25	0.011 869	0.000

The self-consistent nonlocal ($l=0,1,2$) pseudopotential band structure of tungsten is shown in Fig. 9. Some energy eigenvalues at high-symmetry points are collected in Table VI, where they are also compared with the non-self-consistent mented plane waves (APW) results of Mattheiss.[49] The latter have been obtained within the muffin-tin approximation to the superposition density of tungsten atoms in the $3d^5 6s^1$ configuration using an exchange coefficient of $\alpha=1$. These results are virtually identical to the similar APW calculation of Petroff and Viswanathan,[50] which were obtained by superposing atomic densities of the $5d^4 6s^2$ configuration. The agreement between the APW and the present results is fair. A few noticeable discrepancies occur: (i) the s-d splitting (Γ_1-H_{12}, Γ_1-N_1) is substantially smaller in the present calculation (0.18 eV) relative to the APW results (0.75 eV). We find this gap to be very sensitive to the details of the self-consistency (the Γ_1-H_{12} splitting being 0.55 eV in the zeroth iteration in which a superposition pseudocharge-density model is used) as charge is exchanged between the s and the d shells.[51] As the charge density is substantially more localized in the $d_{x^2-y^2}+d_{z^2}$ state at the bottom of the d band (H_{12}) than in the extended s state Γ_1 (see below), one further expects these states to vary differently under exchange scaling leading to a sensitive Γ_1-H_{12} gap. Indeed, Mattheiss[49] found this gap to change by as much as 0.6 eV as the exchange coefficient α is varied from 1.0 to 0.7. The early cellular calculation of Manning and Chodorow[52] leads to results that are similar to the APW results except that the Γ_1-H_{12} gap is negative. (ii) The p-d gap between $N_{1'}(6p)$ and $N_1(5d)$ is close to zero in the APW results, while in the present calculation it is 0.32 eV. This gap is again sensitive to the details of self-consistency and exchange scaling for the same reasons discussed above. Its occurrence constitutes a qualitative difference with respect to molybdenum in which no p-d gap is present.[21,53] This might have direct consequences on the existence of surface states in the corresponding materials as a $N_{1'}$-N_1 gap would persist in the (001)-surface projected band structure (at $\bar{M}$).[54] (iii) The antibonding d state (second $\Gamma_{25'}$) is much separated from its bonding counterpart in the present calculation (24 eV) than in the APW calculation[50] (16 eV), suggesting stronger d-d overlap in the present representation.

TABLE VI. Energy-band eigenvalues (in eV) of tungsten as obtained in the present self-consistent nonlocal pseudopotential calculation and APW (Ref. 49).

State	Present results	APW
Γ_1	0.00	0.00
Γ_{25}	4.80	5.51
Γ_{12}	8.31	8.38
Γ_{25}	28.80	21.37
H_{12}	0.18	0.75
$H_{25'}$	10.44	11.26
$H_{12}-H_{25'}$	10.27	10.51
P_4	3.32	4.16
P_3	9.00	9.41
P_1	15.93	17.66
N_1	0.56	1.28
N_2	2.47	3.28
$N_{1'}$	7.89	8.64
N_1	8.21	8.67
N_4	8.92	9.28
N_3	11.03	12.16

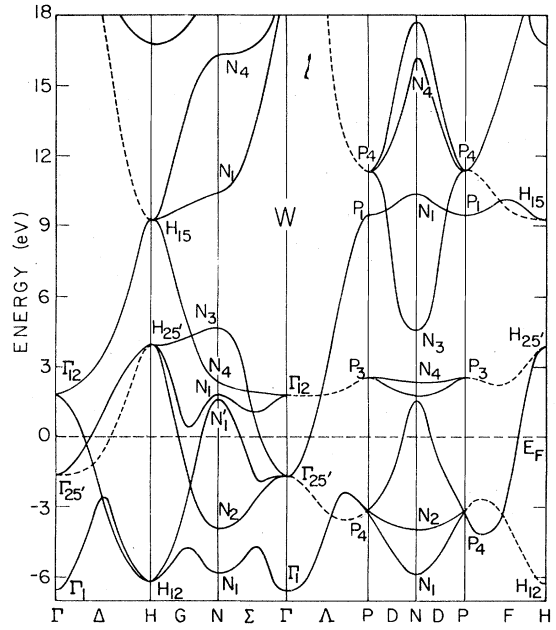

FIG. 9. Self-consistent-exchange and correlation-band structure of tungsten using the nonlocal ($l=0,1,2$) first-principles pseudopotential. Dashed lines denote doubly degenerated representations.

The internal structure of the d band is very similar in the two calculations as these features are rather insensitive in these materials to charge redistribution, exchange scaling[49] or muffin-tin approximations.[55,56] The d-band width is 10.27 eV in the present calculation compared with 10.51 eV in the APW results and similarly the distance of the Fermi energy from the H_{12} bottom of the d band is 6.20 eV in the present calculation and 6.17 eV in APW.

The calculated density of states of tungsten is given in Fig. 10. The general features are very similar to the APW results.[49,50] Three pronounced peaks appear below the Fermi energy, at $\epsilon_F-4.5$

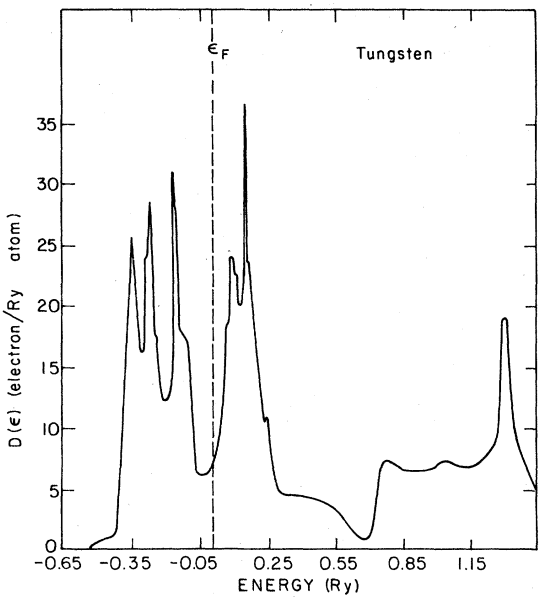

FIG. 10. Density of states of tungsten, obtained from the first-principles pseudopotential calculation.

eV, $\epsilon_F - 3.4$ eV, and $\epsilon_F - 1.6$ eV. These peaks appear at approximately −4.6, −3.3, and −1.8 eV in the calculation of Mattheiss[49] and −4.3, −3.1, and −1.7 eV in the calculation of Petroff and Viswanathan,[50] the differences probably reflecting the more extensive BZ sampling used by the latter authors than genuine differences in the band structure. The three peaks at the occupied part of the density of states originate from predominatly $s + d_{z^2}$, $xy+yz+zx$, and $xy+yz+zx$ states, respectively. The Fermi energy appears at a region of low density of states, followed by a broad structure of about 4 eV which constitutes the unoccupied portion of the d band. This structure shows two pronounced peaks at 1.4 eV (due to p- and d-type states around N_1' and N_1, respectively) and at 2.45 eV (due to the d states around P_3 and N_1+N_4).

The density of states at the Fermi energy $D(\epsilon_F)$ is 6.96 electron/(Ry atom). This is close to the value of ~7.2 electron/(Ry atom) obtained by Petroff and Viswanathan,[50] leading to an electronic specific heat of 3.1×10^{-4} cal/moleK^2, compared with the observed values of 3.10×10^{-4} (Ref. 57) and $(2.5\pm1)\times10^{-4}$ cal/moleK^2.[58]

As relativistic effects are not included in the present calculation, a detailed comparison with the measured Fermi surface cannot be made and only its gross features will be discussed. Figure 11 compares the calculated (110) section of the Fermi surface (broken lines) along with the experimental dimensions (full lines) obtained by Walsh and Grimes[59] using size-effect techniques, the magnetostatic data of Rayne *et al.*,[60] and the de Haas–van Alphen results of Sparlin.[61] The agreement with experiment is generally good. The dimensions of the hole ellipsoid at N are sensitively determined by the location of the p-type N_1' state. As the p-d gap between N_1' and N_1 opens up during the self-consistency iterations, the dimensions of the ellipsoid around N decrease towards their observed values. The hole octahedron at H is very accurately reproduced and so is the electron jack at Γ. The absence of spin-orbit interactions in the present calculation shows up in the absence of a gap between the electron jack and the hole octahedron along Δ.

The nature of the bonding in tungsten can be studied from the variational charge densities. The lowest band at Γ (Γ_1) is a pure 6s-like state whereas one progresses to the next state at Γ we observe the bonding $xy+yz+zx$ state ($\Gamma_{25'}$) which has a background of 6s character. These states are directed predominantly along the nearest-neighbor axis and form the metallic d bond. The lower part of the d band (e.g., $H_{12'}$) contains d_{z^2} and $d_{x^2-y^2}$ nonbonding character that is directed toward the next nearest neighbors and forms a loose bond. As one moves away from the Δ direction, p character is admixed into the bond with increasing proportions at higher energies. The P_4 state at the center of the d band is a combination of d-like $xy+yz+zx$ and the p-like $x+y+z$ representation giving rise to a bond which is directed toward the nearest neighbors with some polarization towards the next nearest neighbors. Just above ϵ_F at the N point (N_1')

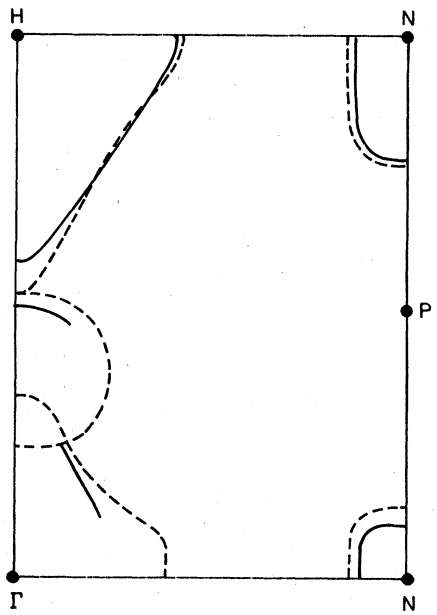

FIG. 11. Calculated (dashed line) and measured (Refs. 59–61) (solid line) dimensions of the Fermi surface of tungsten in the (110) plane.

one encounters a p state. The unoccupied portion of the conduction band is made predominanatly from nonbonding d_{z^2} states (Γ_{12}, P_3, N_1) with x^2-y^2 components slightly admixed. The basic bonding mechanism in tungsten arises from the overlapping bond-directed $xy+yz+zx$ "t_{2g}"-like d states which prevail throughout the zone while s and p bonding have somewhat lower contributions and are concentrated predominantly at the lower and upper parts of the occupied band, respectively. The total valence charge density (Fig. 12) is indicative of such a combination of localized bond directed d-states with a more diffused background contributed by s-p bonding. No accurate experimental x-ray scattering factors are available for this material for comparison with the present calculation.

We next consider the features of the self-consistent valence screening field. Table VII shows the components of the valence Coulomb (V_{Coul}), exchange (V_x), and correlation (V_{corr}) potential in tungsten. It is seen that contrary to the situation encountered in semiconductors (e.g., Si, Sec. II D) only the first reflection is large (i.e., [111]), the rest being usually much smaller. The rate of decay of these small components is, however, considerably slower, due to the localized features of the charge density (1505 plane waves are normally required to expand the total valence density effectively). Both exchange and correlation contributions are seen to screen the Coulomb interactions, with increasing efficiency at higher momenta. As previously observed in Si, the correlation screening is not simply proportional to the exchange screening at low momenta (V_{corr}/V_x varying by as much as a factor of 3 over the first reflections) whereas at high momenta the ratio V_{corr}/V_x is roughly constant ($\simeq 0.05$). This enables an approximate simulation of correlation effects at *high momenta* by artifically increasing the exchange coefficient by 5% (i.e., $\alpha \simeq 0.70$). The last column of Table VII gives for comparison the Fourier components of the $l=0$ pseudopotential. The screening field is seen to be about 10% of the core pseudopotential for the lowest reflection and of the order of 1% for higher reflections. The slow decay of the screened core pseudopotential $[V_{\mathrm{Coul}}+V_x+V_{\mathrm{corr}}+W_l(r)]$ dramatizes the difficulties in describing the electronic properties of these systems within empirical procedures employing truncated pseudopotential form factors.

III. APPLICATION TO CRYSTAL-PHASE SEPARATIONS

A. Orbital radii and valence properties

As the valence electronic structure near the Fermi energy is determined primarily by relatively-low-momentum scattering events, it has been possible in the past successfully to describe the one-electron optical spectra and the Fermi surface of many solids[2] assuming conveniently truncated model pseudopotentials with $q_{\max} \lesssim 3\vec{k}_F$ (i.e., smoothly varying near the core region). The freedom hence offered by the insensitivity of the dispersion relation $\epsilon_j(\vec{k})$ to the repulsive nature of the core potential has been exploited[2] to obtain model potentials that are rapidly converged in

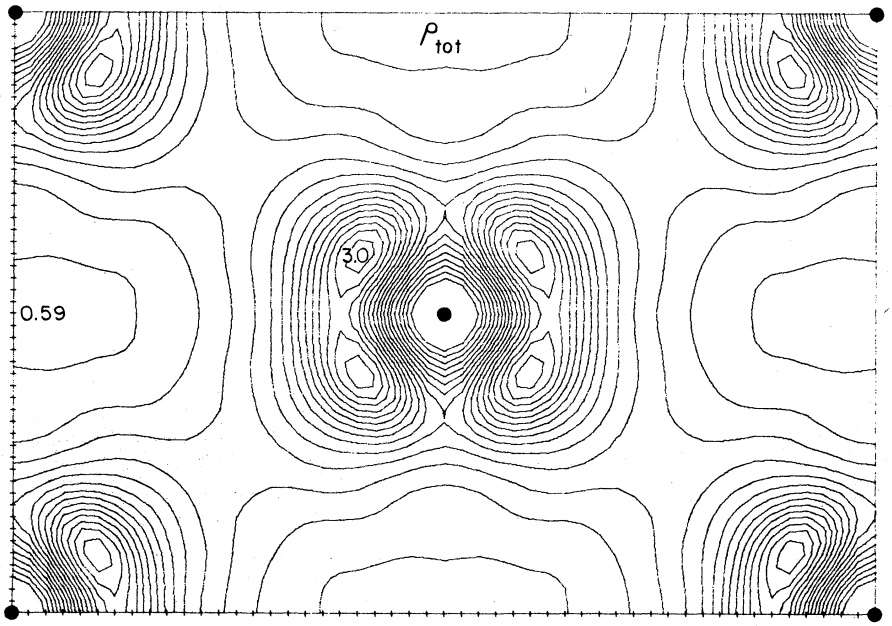

FIG. 12. Total valence pseudocharge density in tungsten in the (110) plane. Full dots represent atomic positions. Results are given in e/cell (normalized to unity).

TABLE VII. Fourier components (with respect to individual unsymmetrized plane waves) of the self-consistent pseudocharge density ρ (in units of e/cell) and the Coulomb (V_{Coul}), exchange (V_x), and correlation (V_{corr}) components of the screening field in tungsten. The last Coulomb gives the Fourier components of the $l=0$ core pseudopotential. The origin is taken at the atomic site. The potential is given in Ry.

Star No.	$\rho(\vec{G})$	$V_{\text{Coul}}(\vec{G})$	$V_x(\vec{G})$	$V_{\text{corr}}(\vec{G})$	$V^{\text{PS}}_{l=0}(\vec{G})$
1	6.0000	...	−0.741 00	−0.117 60	...
2	0.6905	0.073 60	−0.025 00	−0.001 29	0.4403
3	−0.0235	−0.001 25	0.004 47	0.000 35	0.4157
4	0.0339	−0.001 20	0.002 84	0.000 14	0.3349
5	−0.0755	−0.002 01	0.003 53	0.000 23	0.2678
6	−0.1755	−0.003 74	0.006 04	0.000 33	0.2157
7	−0.0431	−0.000 77	0.001 63	0.000 11	0.1760
8	−0.0751	−0.001 14	0.002 64	0.000 16	0.1454
15	−0.0113	−0.002 20	0.000 82	0.000 07	0.0538

reciprocal space and hence amenable to perturbative treatments[62] and planewave representations.[2,3] In contrast, the first-principles pseudopotentials are usually characterized by strongly repulsive core components represented by the Pauli potential $U_l(r)$ for l present in the core.[1a,b] This gives rise to zero-energy classical turning points $V(r_l^0)=0$ that occur as a balance between the repulsive Pauli term $U_l(r)$ and the nuclear attraction $-Z_v/r$, modified by screening, core-orthogonality, and exchange-correlation nonlinearity effects.[1a,b] We have seen that although $U_l(r)$ is confined primarily to the core region, it is intimately related to the properties of the wave functions in the valence regions. By way of construction, its repulsive nature is a direct consequence of the constraint of maximum similarity between the smooth pseudo-wave-functions χ and the real wave functions ψ (in the valence region), imposed within the linear relationship of χ and ψ.[1] It is hence not surprising that the l-dependent turning points r_l^0 tend to scale as the valence properties—in much the same way as the radii of minimum potential[1] $r_l^{\min}$, their variation with the position of the atom in the Periodic Table reflects the underlying chemical regularities of the valence states.

Recently, Simons,[63] Simons and Bloch[64] (SB), and St. John and Bloch[65] have observed that if a "hard-core" nonlocal model potential is assumed, instead of the more conventional smooth model semiempirical potentials, its classical turning points r_l^0 form powerful structural indices, capable of separating the various crystal phases of the octet $A^N B^{8-N}$ non-transition-metal compounds. The SB effective potential is

$$V_{\text{eff}}^{(l)}(r)=V_R^{(l)}(r)+V_v(r) \tag{5}$$

with the repulsive part chosen as

$$V_R^{(l)}(r)=B_l/r^2 . \tag{6}$$

Here B_l is an adjustable constant and $V_v(r)$ is the potential due to the valence field. $V_R^{(l)}(r)$ represents the repulsive potential experienced by the valence states having the same angular momentum l as in the core, due to the explicit relaxation of the core-valence orthogonality constraint. When this potential is specialized to the case of a *single-valence-electron system*, the complicated valence-valence interelectronic interactions vanish and $V_v(r)$ is given in the central-field limit as

$$V_v(r)=-Z_v/r+l(l+1)/2r^2 , \tag{7}$$

where Z_v is the valency. As in the early work of Fues,[66] they showed that the eigenvalues ϵ_{nl} of the central field problem associated with $V_{\text{eff}}^{(l)}(r)$ are analytically solvable in terms of B_l, allowing thereby a simple determination of the latter (and the turning points r_l^0) in terms of the observed spectral excitation energies. These are simply given by

$$\epsilon_{nl}=\frac{-Z_v}{2[n-l-\frac{1}{2}+\frac{1}{2}(1+8Z_v r_l^0)^{1/2}]^2} . \tag{8}$$

The realization that these empirical orbital radii $r_l^0=B_l/Z_v+l(l+1)/2Z_v$ are characteristic of the atomic core and as such are transferable to atoms in various bonding situations has led to the construction of a number of new phenomenological relations $G=f(r_l^0)$ that correlate physical observables G in condensed phases with the orbital radii of the constituent atoms. Some examples are the elemental work functions Φ^A given by Chelikowsky and Phillips[67] as

$$\Phi^A=\sum_{l=0}^{2}\frac{a_l}{r_l^0}+b , \tag{9}$$

the melting point T^{AB} of binary AB compounds[67]:

$$T^{AB}=C_0+C_1R_\sigma^{AB}+C_2R_\pi^{AB}+C_3R_\sigma^{AB}R_\pi^{AB} +C_4R_\sigma^{AB}R_\sigma^{AB}+C_5R_\pi^{AB}R_\pi^{AB} , \tag{10}$$

where the structural coordinates R_π^{AB} and R_σ^{AB} are given by[65]

$$R_\pi^{AB} = (r_p^A - r_s^A) + (r_p^B - r_s^B),$$
$$R_\sigma^{AB} = (r_p^A + r_s^A) - (r_p^B + r_s^B). \tag{11}$$

St. John and Bloch[65] have shown that a two-dimensional topological map of R_σ^{AB} vs R_π^{AB} accurately separates the various structural phases of the octet binary compounds including the wurzite-zincblende and diamond-graphite systems. Machlin, Chow, and Phillips[68] have subsequently found that the *same* orbital parameters provide an excellent structural delineation of the suboctet $A^N B^{P-N}$, $3 \leq P \leq 6$ compounds. Further, a least-squares fitting of the forms 9 and 10 to the available experimental data on Φ^A and T_m^{AB} (where a_l, b, and C_1–C_5 are adjustable parameters, independent of the atom) produced very good correlations with the observed values of the work function and melting points.[67] The same authors were able to represent the two phenomenological coordinates of Meidema *et al.*[69] which predict the signs of the heat of formation of about 500 binary alloys using element-dependent adjustable parameters, by using two simple functions $f_1(r_l^0)$ and $f_2(r_l^0)$ in which the only element-dependent parameters are the spectroscopic turning points r_l^0.

What has been realized[64,65,67,68,70,71] is that the essential characteristics of an isolated atomic core, as implicit in the spectroscopically determined anisotropic turning points r_l^0, contain the fundamental constructs which describe the structural systematics in polyatomic systems. This can be contrasted with other phenomenological measures of the "electronegativity" parameters which are based on various observables pertaining to the *polyatomic systems themselves*, (e.g., the thermochemical Pauling scale,[72] the dielectric Phillips–Van Vechten scale,[73] or the Walsh scale,[74] which is related to diatomic vibrational force constants).

Whereas the model potential that have been successfully used for fitting the low-energy electronic band structure of solids[2,3] usually lack turning points (e.g., Fig. 1) and hence cannot be used in the present framework to define structural parameters, the structurally significant Fues-Simons-Bloch ion potentials[63-66] do not yield a quantitatively satisfactory description of the electronic structure of atoms[75] or simple polyatomic systems.[76,77] The reason for that[1a] lies both in the unphysically long range of the repulsive Pauli field B_l/r^2 in the simple analytically solvable model [Eqs. (5)–(7)] and in the fact that the core potentials pertaining to *relaxed* atomic orbitals [e.g., the ions used in fitting Eq. (8) are B^{3+}, C^{3+}, N^{4+}, O^{5+}, etc.] do not adequately describe the valence states of atoms that occur in bonded phases as nearly neutral species. One is hence faced with the situation where the different emphasis of the Fues-Simons-Bloch potential on one hand and the band-structure-derived empirical pseudopotentials[2,3] on the other hand in fitting their corresponding forms in different momentum transfer regimes (the high-$\vec{q}$ and $\vec{q} \approx 2\vec{k}_F$ regions, respectively), results in the lack of a unified approach to electronic properties and structure. We show here that the currently developed first-principles pseudopotentials, which describe well the electronic properties of atoms and solids in the LDF framework, can also be used to separate all the structural phases of both the octet and suboctet binary compounds with an accuracy that is at least as good as that based on the empirical Fues-Simons-Bloch scheme.

B. Construction of orbital radii and comparisons with empirical schemes

We note that the Fues-Simons-Bloch potential (5) and (6) corresponds to the first two terms in our first-principles potential [Eq. (19) in I] where $U_l(r)$ is replaced by its asymptotic form C_l/r^2 [Eq. (21) in I] at small r. However, as $U_l(r)$ decays much faster than r^{-2} in the outer core region,[1a] the first-principles pseudopotential does not lead to unphysically compressed valence wave functions.[1a] The remaining terms in the first-principles potential are related to interelectronic interactions in the valence system and the orthogonality hole effects, which are absent in the single-electron representation used by SB. As discussed in I, these are important in producing an accurate description of the electronic structure in *many-electron* systems such as atoms or solids.

In order to define generalized core radii that can be used as nearly system-invariant transferable quantities one has to assess the importance of the (system-dependent) screening effects on the turning points of the potential. As the pseudopotential approach replaces the all-electron potential (N_{tot} electrons) by a sum of a static core potential $W_l(r)$ (replacing the effects of N_c core electrons) and a dynamic valence screening field $V_v(r)$ (representing the interactions of N_v valence electrons), the properties of $W_l(r)$, including its turning points, would clearly depend on the choice of $N_c = N_{\text{tot}} - N_v$. We have previously indicated[1] that there are few equally plausible divisions of N_{tot} into the subsets N_c and N_v; the decision is normally dictated by the assumed passivity of a certain core subspace towards external perturbations of interest. Hence while the $3d$, $4d$, and $5d$ orbitals are viewed as valence states for atoms at the center portion of rows 3, 4, and 5, respectively, they can be treated as a part of the inert core towards the end of these

rows for the purpose of studying their low-energy valence spectra. Clearly, any physically significant pseudopotential structural parameter should not depend on the arbitrary assignment of N_c and N_v. We find that the *screened* potential $V_{\rm eff}^{(l)}(r)$ is, however, invariant under the redefinition of the core-valence subspaces (for fixed outer valence states). The reduction of N_c in favor of N_v produces deeper core potentials due to the reduced kinetic energy cancellation and this is counterbalanced by the enhanced screening of the increased valence subspace. Numerically, we find that whereas the turning points r_0 and r_1 of the *core potential* of Zn change from 0.74 and 0.86 a.u., respectively, when the $3d$ orbitals are treated as core, to 0.44 and 0.47 a.u. when the $3d$ orbitals are treated as a valence state, the radii r_0 and r_1 of the *screened (effective) core potentials* are 0.82 and 1.06 a.u., respectively, for both partitioning schemes. Further, we find that the screened potential radii are insensitive to the particular choice of valence configuration (e.g., changing from an s^2p^2 to an s^1p^3 configuration in column-IV atoms or from $s^2p^3d^0$ to $s^1p^3d^1$ in Ge and As, etc.) to within about 0.01 a.u. and hence can be meaningfully used as transferable parameters.

The core radii determined from the screened first-principles potentials are given in Table VIII. Self-interaction corrections[1a] have been included for the single-valence-electron alkali atoms (using a $s^{0.5}p^{0.5}$ configuration). The s and p radii of the nontransition elements are depicted graphically in Figs. 13 and 14 according to their position along rows. In general, r_l^0 contracts with increasing valence charge Z_v for any row in the Periodic Table (left to right in Figs. 13 and 14) due to core-attraction effects and expands with the core charge Z_c (from the lower to the upper part of Figs. 13 and 14) due to the improved pseudopotential cancellation associated with the increased core. The regularities of r_l^0 are qualitatively similar to those of the minimum potential radii $r_l^{\rm min}$ discussed in I and will not be repeated here.

The reciprocal classical turning points r_l^{-1} scale linearly with some of the conventional electronegativity schemes. Indeed the idea of an electronegativity parameter of pure Coulombic nature dates back to Gordy,[70] who proposed the scale $Z_{\rm eff}/R_c$ where $Z_{\rm eff}$ is the effective charge experienced by a valence electron at the covalent bond radius R_c. The idea of assigning a direct *orbital* character to the electronegativity was first pioneered by Mulliken in the thirties.[71] The currently developed radii offer a simple generalization of these ideas to directly incorporate the anisotropy of the valence states (i.e., angular-momentum dependence) into an electronegativity scale. The quantity r_l^{-1} forms here a direct measure of the scattering power of a screened atomic core towards valence electrons with a given angular momentum character. It is easily seen that r_l^{-1} is directly proportional to the energy eigenvalue ϵ_{nl} [cf. Eq. (8)]. We note

TABLE VIII. Values (in atomic units) of the classical crossing points $W_{\rm eff}(r_l)=0$ of the first-principles screened ground-state pseudopotential (r_s, r_p) and the stripped-ion Simons-Bloch empirical potential $(r_s^{\rm SB}, r_p^{\rm SB})$ (Refs. 63, 64, and 67). Interpolated values are denoted by asterisks.

Element	r_s	r_p	$r_s^{\rm SB}$	$r_p^{\rm SB}$
Li	0.985	1.465	0.465	0.94
Be	0.64	0.44	0.315	0.465
B	0.48	0.315	0.24	0.31
C	0.39	0.25	0.19	0.235
N	0.33	0.21	0.16	0.19
O	0.285	0.18	0.14	0.16
F	0.25	0.155	0.12	0.135
Ne	0.22	0.14	...	...
Na	1.10	1.78	0.51	1.18
Mg	0.90	1.13	0.43	0.715
Al	0.77	0.90	0.37	0.54
Si	0.68	0.74	0.33	0.445
P	0.60	0.64	0.295	0.38
S	0.54	0.56	0.265	0.33
Cl	0.50	0.51	0.245	0.295
Ar	0.46	0.46	...	...
K	1.54	2.15	0.68	1.38
Ca	1.32	1.68	0.61	0.935
Cu	0.88	1.16	0.215	0.805
Zn	0.82	1.06	0.32	0.61
Ga	0.76	0.935	0.33	0.52
Ge	0.72	0.84	0.32	0.46
As	0.67	0.745	0.31	0.415
Se	0.615	0.67	0.295	0.38
Br	0.58	0.62	0.275*	0.37*
Kr	0.56	0.60	...	...
Rb	1.67	2.43	0.725	1.475
Sr	1.42	1.79	0.68	1.045
Ag	1.045	1.33	0.225	0.83
Cd	0.985	1.23	0.355	0.66
In	0.94	1.11	0.38	0.585
Sn	0.88	1.00	0.38	0.535
Sb	0.83	0.935	0.36	0.485
Te	0.79	0.88	0.345	0.445
I	0.755	0.83	0.33*	0.425*
Xe	0.75	0.81	...	...
Cs	1.71	2.60	0.81	1.59
Ba	1.515	1.89	0.775	1.17
Au	1.21	1.45	0.13	0.70
Hg	1.07	1.34	0.30	0.63
Tl	1.01	1.22	0.345	0.58
Pb	0.96	1.13	0.36	0.545
Bi	0.92	1.077	0.36	0.51
Po	0.88	1.02	0.355*	0.49*
At	0.85	0.98	0.345*	0.45*
Rn	0.84	0.94	...	...

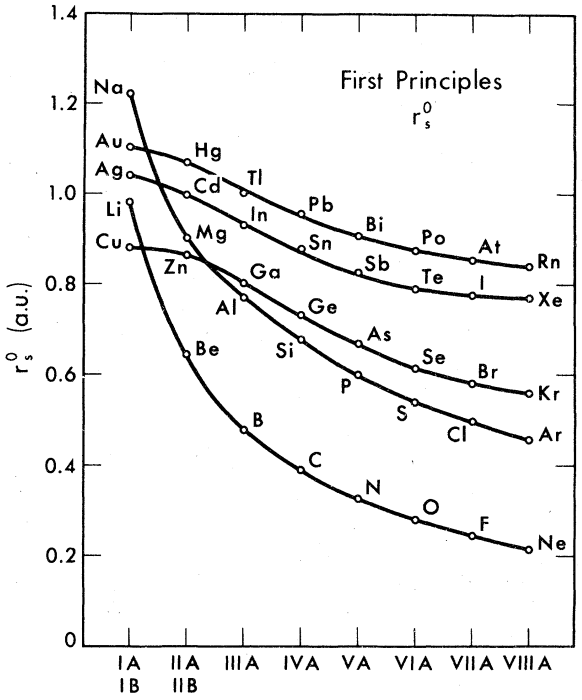

FIG. 13. $l=0$ classical turning points of the screened pseudopotential along rows in the Periodic Table.

that this is in line with the suggestion of Slater[78] that the energy eigenvalues of a local-density Hamiltonian form a sensitive electronegativity scale in that they dictate the flow of charge towards the sites characterized by a lower available unoccupied state. Our present treatment, based on a pseudopotential transformation of the all-electron local density Hamiltonian, expresses these energy-eigenvalue electronegativities in terms of the turning points r_l.

Although the general trends in r_l^0 are similar to those obtained with the empirical Simons-Bloch potential,[64,67] (Table VIII), important quantitative differences are apparent. Our $l=0$ radii for the first-row atoms are about a factor of 2 larger than the SB radii whereas the $l=1$ radii are equal to within a few percent. For atoms from the second row, the present $l=0$ radii are still about a factor of 2 larger but the correlation with the $l=1$ radii is lost. The ratio between the present radii and the SB values for the noble metals Ag and Au is 4.64 and 9.31 for $l=0$ and 1.60 and 2.07 for $l=1$. As the experimental term values for Br^{6+}, I^{6+}, Po^{5+}, and At^{6+} are incomplete, the corresponding SB radii had to be obtained by extrapolation.[67] Similarly, no empirical radii were obtained for transition metals as the spectra of the corresponding single valence electron ions is largely unavailable. In general, the currently developed radii cover a larger range for all angular momenta and show greater separation between the various rows.

Note that whereas the present s and p radii for Cu are smaller than the corresponding radii for both Ag and Au, the empirical SB scheme yields the order $r_l^{Ag} > r_l^{Cu} > r_l^{Au}$ for all $l=0$, 1, and 2. As the empirical $l=2$ radii for these elements ($r_2^{Cu}=2.945$ a.u., $r_2^{Ag}=2.950$ a.u., and $r_2^{Au}=2.935$ a.u.) are equal to within 0.5%, only the variations in the s and p radii along this series are responsible in the SB scheme for the special ordering of the corresponding solid phase work functions [vis. the correlation $\Phi \sim \sum_l r_l^{-1}$ in Eq. (9)] and electronegativities: $\Phi_{Au} > \Phi_{Cu} > \Phi_{Ag}$. In contrast, the present first-principles scheme shows a much larger variation in both the s,p and in particular in the d radii: $r_2^{Cu}=0.185$ a.u., $r_2^{Ag}=0.39$ a.u., and $r_2^{Au}=0.49$ a.u. (for $3d$, $4d$, and $5d$, respectively). The above order of Φ would result in the present scheme from the variations in the nature of the valence d electrons in these systems. Indeed the character of the valence d electrons changes substantially in this series (Cu lacking any core states of $l=2$ symmetry) as also reflected in the corresponding d-orbital kinetic energies per

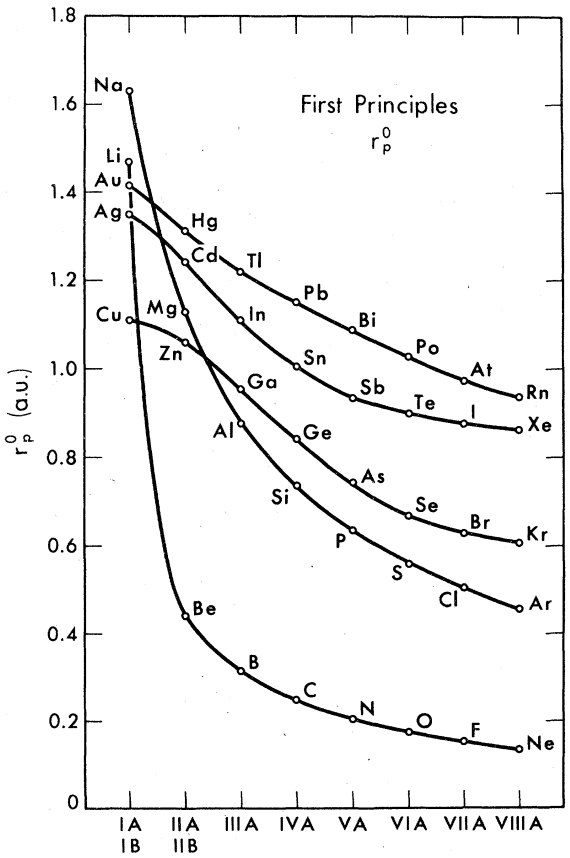

FIG. 14. $l=1$ classical turning points of the screened pseudopotential along rows in the Periodic Table.

electron: $r_{Cu}=9.131$ a.u., $r_{Ag}=7.813$ a.u., and $r_{Au}=8.171$ a.u. It would seem that many of the variations in the properties of the monovalent Cu, Ag, and Au compounds are better rationalized in terms of the underlying differences in the properties of the outer metal d electrons rather than the s and p electrons (e.g., the optical and photoemission properties of CuCl, AgCl, and AuCl showing the interchange of the order of the metal derived d valence subband with the halogen-derived p-valence subband and the rapid decrease in the metal–d-nonmetal s,p hybridization along this series). The failure of the Simons-Bloch scheme to adequately reflect the variations in the properties of the d electrons of the Cu-Ag-Au series in r_2 is related to its confinement to treat *single valence electron systems* [viz. Eq. (7)]. Consequently, the outer $3d$, $4d$, and $5d$ electrons in Cu, Ag, and Au, respectively, *are considered as a part of the inert core* and the r_2 coordinate is fixed from the spectroscopic term values pertaining to excitations into the lowest *unoccupied* $4d$, $5d$, and $6d$ levels, respectively. The near constancy of the empirical r_2 values in the Cu-Ag-Au series hence reflects the properties of the *virtual* d orbitals that have a lesser bearing on the d bonding in the related noble-metal systems than the *valence* d states. As the present first-principles scheme includes directly valence-valence interelectronic interactions, it is not restricted to single-electron models and the occupied d electrons are treated as (dynamic) valence states. Note also that the restriction of the SB scheme to single-valence-electron systems poses a severe problem in treating transition metal elements.

Recently, Andreoni *et al.*[75] have attempted to remedy the deficiency of the SB potential in describing correctly the ionic wave functions by exponentially damping the repulsive B_l/r^2 term in (6). The new repulsive term $V_R^{(l)}(r)=A_l e^{-\gamma_l r}/r^2$ has been fitted (varying A_l and γ_l) to both the ionic term values and the HF stripped ion orbitals. As the latter were available only for the first-row ions, the resulting radii could not be used to examine structural regularities. Their radii for the first-row atoms are, however, similar to the currently developed radii, their $l=0$ values being 1.01, 0.66, 0.49, 0.39, 0.33, 0.28, 0.25, and 0.22 for Li to Ne, compared with the present results of 0.985, 0.64, 0.48, 0.39, 0.33, 0.285, 0.25, and 0.22. For $l=1$ their radii are 0.84, 0.41, 0.28, 0.22, 0.18, 0.15, 0.13, and 0.12 compared with the present results of 1.46, 0.44, 0.315, 0.25, 0.21, 0.155, and 0.14. The origin of these similarities can be understood by comparing the behavior of the repulsive potentials in the two approaches. We show in Fig. 15 the variation of $r^2V_R(r)$ for the alkali atoms. The regular SB model [Eq. (6)] mim-

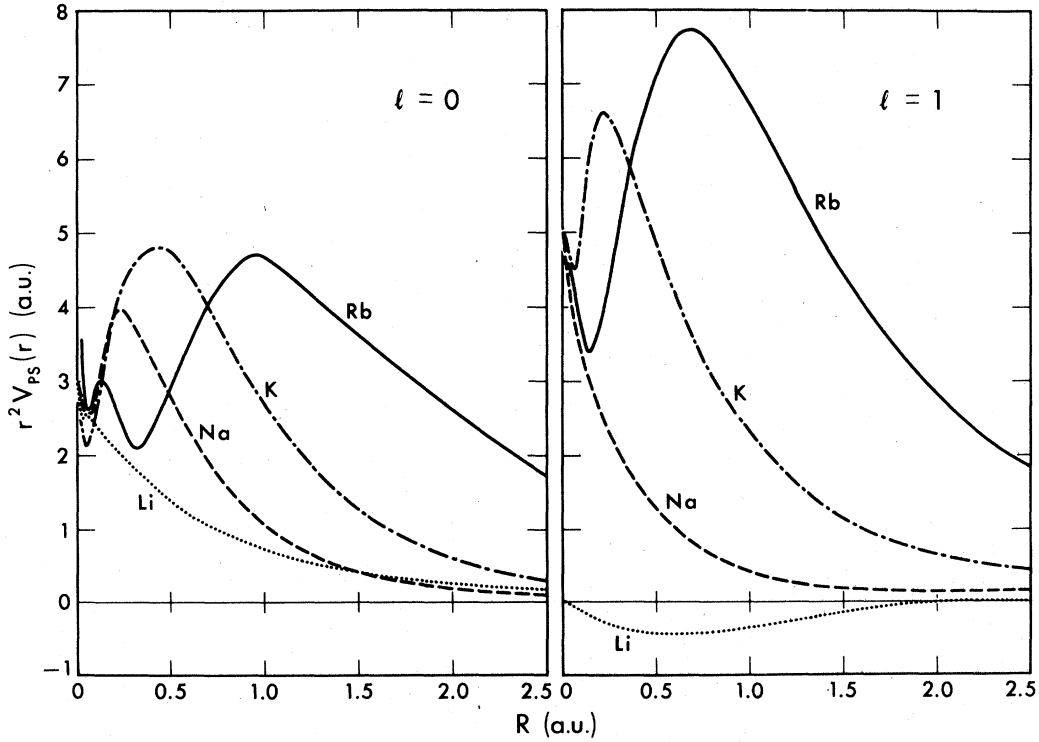

FIG. 15. Plot of $r^2V_R(r)$ for the $l=0$ and $l=1$ symmetries in the alkali atoms, where $V_R(r)$ is the first-principles pseudopotential, excluding the $-Z_v/r$ part.

ics this behavior by a constant line $r^2V_R^{(l)}(r)=B_l$ while the modification of Andreoni *et al.*[75] yields $r^2V_R^{(l)}(r)=A_le^{-\gamma_l r}$ for this function. As the first-principles-derived $r^2U_l(r)$ function decays exponentially in the outer core region (Fig. 15), the latter approximation seems valid. Quantitative differences occur, however, both in the inner core region (where the present results are nonmonotonic due to the shell structure of the real core) and in the values of A_l and γ_l necessary to fit the present results in the outer core region. The latter discrepancy (which is more noticeable for $l=1$) stems directly from the differences between the Z_v-1 ionized wave functions used by Andreoni *et al.*[75] and the neutral ground-state wave functions used in the present study. As we have indicated before, we feel that the latter are more appropriate to describe realistic pseudopotentials for molecules and solids. As the ground electronic state of solids and molecules is largely determined by the configuration interaction between the multiplets of the constituent *atoms* induced by the interelectronic interactions in the lower symmetry polyatomic system (e.g., those arising from the s^2p^2, s^1p^3, etc., for carbon), the highly excited ^2S configuration of the Z_v-1 *ion* does not characterize the ground state of the polyatomic system. One would further expect that as the average of the neutral atom multiplet yields lower ionization and excitation energies than those obtained for the stripped ion, larger equivalent orbital radii [viz. Eq. (8)] would result. This is indeed borne out by the comparison of the SB and the Andreoni *et al.* radii with the present result. However, as these multiplet corrections are similar along columns (due to the same number of valence electrons and smoothly varying coupling coefficients), it would seem reasonable to expect that the regularities in the SB radii would parallel those obtained for neutral atoms.

The empirical approach to orbital radii enjoys the following advantages over the first-principles radii: (i) the radii are determined as easily for light and heavy elements, whereas the determination of the first-principles potential is increasingly more time consuming as the atomic number increases; (ii) implicit in the construction of the empirical potentials are effects that are absent in the presently developed potentials such as relativistic corrections [although limited by the L-S coupling from underlying (6)] and core polarization effects. The latter are apparent from the small nonzero values obtained for B_l even for states that have no matching symmetry in the core (e.g., $2p$ for first-row atoms). In contrast, $U_l(r)$ is identically zero for such cases due to the absence of pseudopotential cancellation.

C. Phase separation in the orbital-radii model

Following St. John and Bloch[65] we have constructed a topological R_π vs R_σ [Eq. (9)] map for 77 of the octet AB compounds (Fig. 16). A similar map has been constructed for 56 suboctet compounds (A^NB^{P-N}, $3\leq P\leq 6$, Fig. 17). Only the most stable forms are included.

It is seen that these coordinates separate remarkably well all the crystal phases involved, including the most sensitive wurzite and zinc-blende phases (which differ only in third-nearest neighbors). Among the notable exceptions we observe that CuF appears near the wurzite-rocksalt line while it was thought to crystallize in a zinc-blende form. A recent reexamination of the data[67] has suggested that this compound does not exist in fact in its stable phase as a AB structure.

The general pattern of phase separation is similar to that obtained by St. John and Bloch[65] and Chelikowsky and Phillips[67] with the empirical radii. Some of the notable differences are: (i) The present scheme places the Cu and Ag halides near the zinc-blende-wurzite-rocksalt border in their appropriate places, whereas the empirical scheme

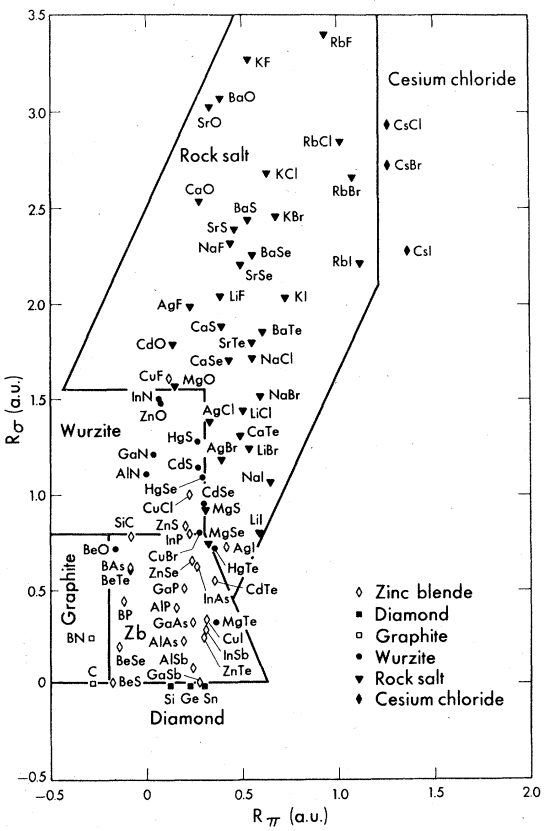

FIG. 16. R_π^{AB} vs R_σ^{AB} plot for the octet AB compounds, obtained with the first-principles pseudopotentials.

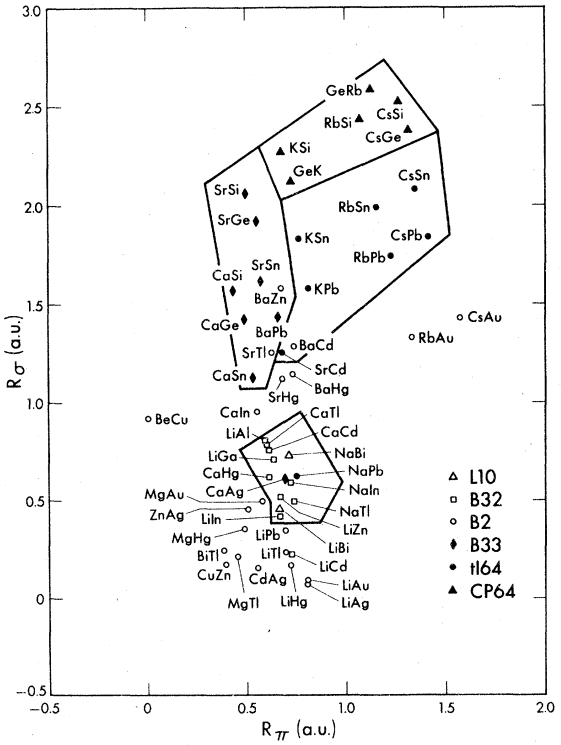

FIG. 17. R_π^{AB} vs R_σ^{AB} plot for the suboctet AB compounds, obtained with the first-principles pseudopotentials.

places them as a nearly separated group at high R_π values. (ii) The empirical R_π coordinate shows only a very small separation of the sulphides, selenides and tellurides of Sr, Cd, Zn, Mg, and Be, and the (extrapolated) R_π values do not separate the bromides from the iodides of Li, Na, K, Rb, Ag, and Cu. This can be viewed from Fig. 18(a) where the corresponding R_π coordinates are plotted for these series. In general, the slopes of the corresponding curves and their separation is distinctly higher with the present radii, indicating larger structural sensitivity. Similarly, the empirical radii place the silver and copper halides between the alkali halides on the R_π scale, while in the present scale they are more logically placed as a separated group. Both these R_π curves and similar R_σ curves indicate that the empirical parameters of Cu and Ag compounds are nearly degenerate. A plot of $r_p - r_s$ vs $r_p + r_s$ for these elements shows approximate linear dependence. To a lesser extent a similar effect characterizes the Cd-Zn pair. (iii) The empirical R_π coordinate places the Mg chalcogenides [Fig. 18(b)] which are mostly rocksalt, below the Zn and Cd chalcogenides (mostly wurzite and zinc blende). The present scale places the Mg chalcogenides closer to the rocksalt Sr salts.

The R_π coordinate measures the sum of the s-p pseudopotential nonlocalities for the pair A-B. Indeed the electronic band structure of many of the compounds characterized by small R_π (e.g., GaAs, AlAs, Si, Ge, ZnSe, etc.) has been treated successfully by local pseudopotentials.[2] It is also a measure of the s-p promotion energies in elemental semiconductors and insulators (e.g., $R_\pi^C < R_\pi^{Si} < R_\pi^{Ge} < R_\pi^{Sn}$) as the difference $r_s^{-1} - r_p^{-1}$ is proportional to $\epsilon_s - \epsilon_p$. R_π correlates successfully with the inverse of the homopolar dielectric gap E_h^{-1},[67] whereas R_σ correlates well with the ionic dielectric gap C.[67]

The R_π vs R_σ map for the suboctet compounds (Fig. 17) separates not only the two broad group of bcc-like structures (full symbols) and anion valence coordination compounds (open circles) but also works well for most of the individual space groups considered. Of the notable exceptions, CaAg($B33$) and NaPb($tl64$) have special properties.[67] The region of intermixing of the $B32$ and $B2$ structures which occurs in the empirical separation map of Machlin *et al.*,[78] is largely eliminated with the present scale.

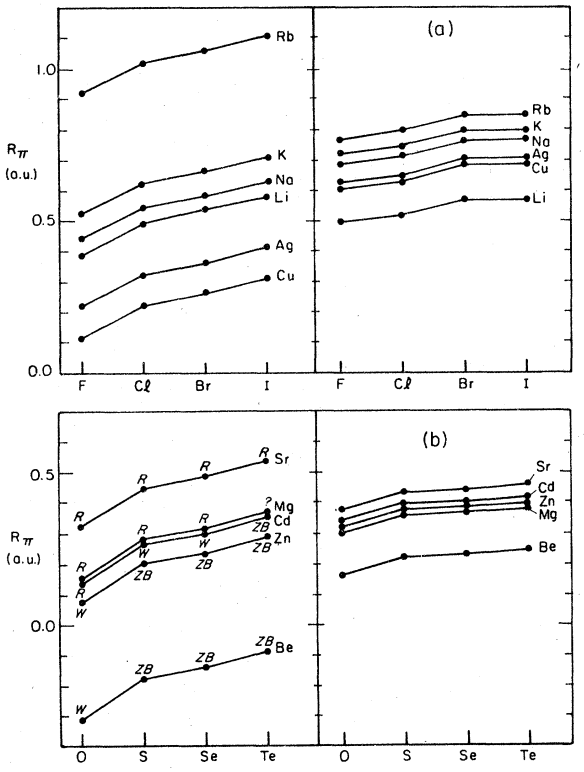

FIG. 18. Variation of the R_π coordinates of the empirical Simons-Bloch (right-hand panels) and the first principles pseudopotential (left-hand panels) along (a) the monovalent halides and (b) the divalent chalcogenides. The symbols R, W, and ZB indicate rocksalt, wurzite, and zincblende, respectively.

The R_σ coordinate has been shown to correlate successfully with the deviations Δ from the ideal c/a ratio (1.633) in wurzite structures.[67] Using the 20 AB compounds for which crystallographic data exist, given by Lawaetz[79] (Table I in Ref. 79), we obtain a correlation coefficient of -0.702, compared with a correlation of -0.788 obtained from the empirical radii[67] and -0.842 obtained by Lawaetz[79] using the empirical $(e^*C/\hbar\omega_p)^2$ coordinate (where e^*, C, and ω_p are the experimentally deduced effective charge, Phillips's heteropolar gap, and the plasma frequency). In view of the nonempirical nature of our scale and its application to systems that have phases more stable than the wurzite, we view our classification as successful. Based on this correlation, we suggest that HgS, HgSe, HgTe, would have a stable wurzite form. Similar conclusions are borne by their location on the R_σ-R_π map.

IV. CONCLUSIONS

We have demonstrated that the first-principles nonlocal pseudopotentials developed in I not only reproduce the energies and wave-function characteristics of atoms and ions very accurately, but they can also be used to obtain a good description of the electronic structure of solids as diverse as covalent semiconductors and transition metals. In addition, they are shown to contain structural information through their characteristic electronegativity parameters r_l. As these potentials are constructed in a nonempirical fashion, their characteristic features can be conveniently analyzed in terms of the underlying interelectronic interactions. This enables the systematic improvements in the understanding of the interaction model by way of comparison with experiment. Although obtained in numerical form, the knowledge of their limiting behavior at small and large radius enables their accurate fitting to convenient analytical forms such as

$$c_1 r^{-2} e^{-\alpha_1 r} + c_2 r^{-1} e^{-\alpha_2 r} + \sum_{i=3}^{N} C_i e^{-\alpha_i r} - \frac{Z_v}{r}$$

This would allow their use for a wide range of problems including electronic properties and crystal structure.

ACKNOWLEDGMENTS

The authors are grateful to J. R. Chelikowsky, L. Kahn, P. Lam, and G. P. Kerker for helpful discussions. We thank J. C. Phillips for helpful discussions and for sending us preliminary versions of Ref. 67 prior to publication. The authors thank D. R. Hamann for discussions on the DF pseudopotential and its application to Si, as well as for performing an independent test on the Si potential. This work was supported in part by the Division of Basic Energy Sciences, U. S. Department of Energy, and by NSF Grant No. DMR76-20647-A01. One of us (A.Z.) acknowledges support by IBM.

*Present address: Solar Energy Research Institute, Golden, Colorado 80401.

[1] (a) A. Zunger and M. L. Cohen, Phys. Rev. B 18, 5449 (1978). (b) A. Zunger, J. Vac. Sci. Technol. (in press). (c) P. A. Christiansen, Y. S. Lee, and K. S. Pitzer (private communication).

[2] M. L. Cohen and V. Heine, in *Solid State Physics*, edited by H. Ehrenreich, F. Seitz, and D. Turnbull (Academic, New York, 1970), Vol. 24, p. 38; D. Brust, in *Methods in Computational Physics*, edited by B. Alder, S. Fernbach, and M. Rotenberg, (Academic, New York, 1968), Vol. 8, p. 33.

[3] M. L. Cohen, M. Schlüter, J. R. Chelikowsky, and S. G. Louie, Phys. Rev. B 12, 5575 (1975).

[4] A. Redondo, W. A. Goddard, and T. C. McGill, Phys. Rev. B 15, 5038 (1977).

[5] M. Schlüter, J. R. Chelikowsky, S. G. Louie, and M. L. Cohen, Phys. Rev. B 12, 4200 (1975); M. Schlüter, J. R. Chelikowsky, S. G. Louie, and M. L. Cohen, Phys. Rev. Lett. 34, 1385 (1975).

[6] S. G. Louie and M. L. Cohen, Phys. Rev. B 13, 2461 (1976).

[7] S. G. Louie, M. Schlüter, J. R. Chelikowsky, and M. L. Cohen, Phys. Rev. B 13, 1654 (1976).

[8] J. A. Appelbaum and D. R. Hamann, Phys. Rev. B 8, 1777 (1973).

[9] S. Topiol, J. W. Moskowitz, C. F. Melius, M. D. Newton, and J. Jafri, ERDA Report No. C00-3077-105, New York University, 1976 (unpublished); L. R. Kahn and W. A. Goddard, Chem. Phys. Lett. 2, 667 (1968); S. Topiol, M. A. Ratner, and J. W. Moskowitz, Chem. Phys. Lett. 46, 256 (1977).

[10] J. Ihm, S. G. Louie, and M. L. Cohen, Phys. Rev. B 17, 769 (1978).

[11] J. C. Phillips, Solid State Commun. 22, 549 (1977).

[12] V. Heine, in *Solid State Physics*, edited by H. Ehrenreich, F. Seitz, and D. Turnbull (Academic, New York, 1970), Vol. 24, p. 1.

[13] L. R. Saravia and D. Brust, Phys. Rev. 176, 915 (1968); W. Saslow, T. K. Bergstresser and M. L. Cohen, Phys. Rev. Lett. 16, 354 (1966); C. Y. Fong and M. L. Cohen, *ibid* 21, 22 (1968).

[14] E. O. Kane, Phys. Rev. 146, 558 (1966).

[15] D. Weaire, in Ref. 12, Vol. 24, p. 250.

[16] R. C. Chaney, C. C. Lin, and E. E. Laforn, Phys. Rev. B 3, 459 (1971); J. E. Simmons, C. C. Lin, D. F. Fouquet, E. E. Lafon, and R. C. Chaney, J. Phys. C 8, 1549 (1975); J. Callaway and J. L. Fry, in *Computational Methods in Band Theory*, edited by P. M. Marcus,

J. F. Janak, and A. R. Williams (Plenum, New York, 1971), p. 512.
[17]A. Zunger and A. J. Freeman, Phys. Rev. B 15, 4716 (1977).
[18]D. E. Ellis and G. S. Painter, Phys. Rev. B 2, 7887 (1970); H. Sambe and R. H. Felton, J. Chem. Phys. 62, 41 (1975).
[19]A. Zunger and M. Ratner, Chem. Phys. 30, 423 (1978).
[20]A. Zunger, S. Topiol, and M. Ratner, Chem. Phys. 38, 75 (1979).
[21]A. Zunger, G. Kerker, and M. L. Cohen, Phys. Rev. B 20, 581 (1979).
[22]S. G. Louie, K. M. Ho and M. L. Cohen, Phys. Rev. B 19, 1774 (1979); R. N. Euwema, Phys. Rev. B 4, 4332 (1971); A. B. Kunz, Phys. Lett. A 27, 401 (1968).
[23]P. O. Löwdin, J. Chem. Phys. 19, 1396 (1951); D. Brust, Phys. Rev. 134, A1337 (1964).
[24]G. Lehman and M. Taut, Phys. Status Solidi 54, 469 (1971).
[25]W. Kohn and L. Sham, Phys. Rev. 170, 1133 (1965).
[26]K. S. Singwi, A. Sjölander, M. P. Tosi, and R. H. Land, Phys. Rev. B 1, 1044 (1970).
[27]D. J. Stukel and R. N. Euwema, Phys. Rev. B 1, 1635 (1970); P. M. Racch, R. N. Euwema, D. J. Stukel, and T. C. Collins, Phys. Rev. B 1, 756 (1970).
[28]The SESCL results in Table I were obtained by the present authors from the potential of Ref. 3 (cf. Fig. 1, dot-dashed line) using an exchange coefficient of $\alpha = 2/3$. This is to be distinguished from the local *empirical* Si potential [i.e., M. L. Cohen and T. K. Bergstresser, Phys. Rev. 141, 789 (1966)] used also in Ref. 29, which is given as a parametrized *effective* potential and hence cannot be made self-consistent.
[29]J. R. Chelikowsky and M. L. Cohen, Phys. Rev. B 10, 5095 (1974).
[30]W. E. Spicer and R. C. Eden, in *Proceedings of the Ninth International Conference of the Physics of Semiconductors, Moscow, 1968* (Nauka, Leningrad, 1968), Vol. 1, p. 61.
[31]W. D. Grobman and D. E. Eastman, Phys. Rev. Lett. 29, 1508 (1972).
[32]L. Ley, S. Kowalcyzk, R. Pollak, and D. A. Shirley, Phys. Rev. Lett. 29, 1088 (1972).
[33]M. Walkowsky and R. Braunstein, Phys. Rev. B 5, 497 (1972); R. R. L. Zucca, J. P. Walter, Y. R. Shen, and M. L. Cohen, Solid State Commun. 8, 627 (1970).
[34]K. M. Ho, M. L. Cohen, and M. Schlüter, Chem. Phys. Lett. 46, 608 (1977).
[35]Y. W. Yang and P. Coppens, Solid State Commun. 15, 1555 (1974).
[36]A. Zunger and A. J. Freeman, Phys. Rev. B 15, 5049 (1977).
[37]D. J. Miller, D. Haneman, E. J. Baerends and P. Ross, Phys. Rev. Lett. 41, 197 (1978).
[38]M. Schlüter, A. Zunger, G. P. Kerker, K. M. Ho and M. L. Cohen, Phys. Rev. Lett. 42, 540 (1979).
[39]D. J. Chadi and M. L. Cohen, Phys. Rev. B 7, 692 (1972); H. J. Monkhorst and J. D. Pack, ibid 13, 5188 (1976).
[40]J. C. Slater, *The Self-Consistent Field for Molecules and Solids* (McGraw-Hill, New York, 1974), p. 35.
[41]A. Zunger and A. J. Freeman, Phys Rev. B 16, 2901 (1977).
[42]A. Zunger and A. J. Freeman, Phys. Rev. B 17, 4850 (1977).
[43]R. N. Euwema and L. R. Kahn, J. Chem. Phys. 66, 306 (1977).
[44](a) H. Hattori, H. Kuriyama, T. Katagawa, and J. N. Kato, J. Phys. Soc. Jpn. 20, 988 (1965); M. Hart and A. D. Milne, Acta Crystallogr. A 25, 134 (1969); (b) P. J. E. Aldred and M. Hart, Proc. R. Soc. Lond. A 332, 223 (1973); P. Trucano and B. W. Batterman, Phys. Rev. B 6, 3659 (1972).
[45]C. B. Haselgrove, Math. Comput. 15, 373 (1961).
[46]F. Herman, in *Proceedings of the Second International Conference on the Physics of Semiconductors, Paris, 1964* (Dunod, Paris, 1964), p. 3.
[47]J. R. Chelikowsky and M. L. Cohen, Phys. Rev. B 14, 556 (1976).
[48]F. Herman, R. L. Kortum, C. D. Kuglin, and S. Skillman, in *Methods of Computational Physics*, edited by B. Alder, S. Fernbach, and M. Rotenbert (Academic New York, 1968), Vol. 8, p. 193.
[49]L. F. Mattheiss, Phys. Rev. 139, 1893 (1965).
[50]I. Petroff and C. R. Viswanathan, Phys. Rev. B 4, 799 (1971).
[51]By means of self-consistent atomic calculations we find that the free-atom s–d splitting decreases to 0.21 eV as the atom undergoes a transition between the d^4s^2 to the d^5s^1 configuration. As the atoms are overlapped in this frozen configuration to form a crystal, the splitting increases to 0.55 eV (predominately due to volume renormalization effects) and the order of s and d states reverses relative to the free atom (i.e., the d state moves to be above the s state). Further charge redistribution in the solid introduced through self-consistency acts to diminish the s–d splitting to about 0.2 eV.
[52]M. F. Manning and M. I. Chodorow, Phys. Rev. 56, 789 (1939).
[53]D. D. Koelling, F. M. Mueller, A. J. Arko, and J. B. Ketterson, Phys. Rev. B 10, 4889 (1974).
[54]G. P. Kerker, K. M. Ho, and M. L. Cohen (unpublished).
[55]E. Elyashar and D. D. Koelling, Phys. Rev. B 13, 5362 (1976).
[56]G. S. Painter, J. S. Faulkner, and G. M. Stocks, Phys. Rev. B 9, 2448 (1974).
[57]*Handbook of Chemistry and Physics*, 48th ed., edited by R. C. Weast (Chemical Rubber, Cleveland, Ohio, 1968), p. 100.
[58]R. R. Hultgren, R. L. Orr, P. D. Anderson, and K. K. Kelly, in *Selected Values of Thermodynamic Properties of Metals and Alloys* (Wiley, New York, 1963), p. 176.
[59]W. M. Walsh and C. C. Grimes, Phys. Rev. Lett. 13, 523 (1964).
[60]J. A. Rayne and H. Sell, Phys. Rev. Lett. 8, 149 (1962), J. A. Rayne, Phys. Rev. 133, 1104 (1964).
[61]D. M. Sparlin, Ph.D. thesis (Northwestern University, 1964) (unpublished).
[62]W. A. Harrison, *Pseudopotentials in the Theory of Metals* (Benjamin, New York, 1966).
[63]G. Simons, J. Chem. Phys. 55, 756 (1971); Chem. Phys. Lett. 12, 404 (1971).
[64]G. Simons and A. N. Bloch, Phys. Rev. B 7, 2754 (1973).
[65]J. St. John and A. N. Bloch, Phys. Rev. Lett. 33, 1095 (1974).
[66]E. Fues, Ann. Phys. (Leipz.) 80, 367 (1926).

[67]J. R. Chelikowsky and J. C. Phillips, Phys. Rev. B 17, 2453 (1978); Phys. Rev. Lett. 39, 1687 (1977).
[68]E. S. Machlin, T. P. Chow, and J. C. Phillips, Phys. Rev. Lett. 38, 1292 (1977).
[69]A. R. Miedema, F. R. de Boer, and P. F. de Chatel, J. Phys. F 3, 1558 (1973) and references therein.
[70]W. Gordy, Phys. Rev. 69, 604 (1946).
[71]R. S. Mulliken, J. Chem. Phys. 2, 782 (1934).
[72]L. Pauling, *The Nature of the Chemical Bond* (Cornell U. P., Ithaca, 1960).
[73]J. C. Phillips and J. A. Van Vechten, Phys. Rev. B 2, 2147 (1970).
[74]A. D. Walsh, Proc. R. Soc. Lond. A 207, 13 (1951).
[75]W. Andreoni, A. Baldareschi, F. Meloni, and J. C. Phillips, Solid State Commun. 24, 245 (1978).
[76]G. Simons, Chem. Phys. Lett. 18, 315 (1973); 12, 404 (1971).
[77]J. C. Barthelat and P. Durand, Chem. Phys. Lett. 16, 63 (1972); P. Durand and J. C. Barthelat, *ibid.* 27, 191 (1974).
[78]J. C. Slater, in Ref. 40, p. 94; Int. J. Quantum Chem. 3S, 727 (1970).
[79]P. Lawaetz, Phys. Rev. B 5, 4039 (1972).